A&A 478, 335–351 (2008)
DOI: 10.1051/0004-6361:20078663

Astronomy & Astrophysics

Evolution of chemical abundances in Seyfert galaxies

S. K. Ballero[1,2], F. Matteucci[1,2], L. Ciotti[3], F. Calura[2], and P. Padovani[4]

[1] Dipartimento di Astronomia, Università di Trieste, via G.B. Tiepolo 11, 34143 Trieste, Italy
e-mail: ballero@oats.inaf.it
[2] INAF, Osservatorio Astronomico di Trieste, via G.B. Tiepolo 11, 34143 Trieste, Italy
[3] Dipartimento di Astronomia, Università di Bologna, via Ranzani 1, 40127 Bologna, Italy
[4] European Organisation for Astronomical Research in the Southern Hemisphere (ESO), Karl-Schwarzschild-Str. 2, 85748 Garching bei München, Germany

Received 12 September 2007 / Accepted 23 October 2007

ABSTRACT

Aims. We study the chemical evolution of spiral bulges hosting Seyfert nuclei, based on updated chemical and spectro-photometrical evolution models for the bulge of our Galaxy, to make predictions about other quantities measured in Seyferts and to model the photometric features of local bulges. The chemical evolution model contains updated and detailed calculations of the Galactic potential and of the feedback from the central supermassive black hole, and the spectro-photometric model covers a wide range of stellar ages and metallicities.

Methods. We computed the evolution of bulges in the mass range $2 \times 10^9 - 10^{11}$ $M_\odot$ by scaling the efficiency of star formation and the bulge scalelength, as in the inverse-wind scenario for elliptical galaxies, and by considering an Eddington limited accretion onto the central supermassive black hole.

Results. We successfully reproduced the observed relation between the masses of the black hole and of the host bulge. The observed nuclear bolometric luminosity emitted by the supermassive black hole is reproduced only at high redshift or for the most massive bulges; in the other cases, a rejuvenation mechanism is necessary at $z \simeq 0$. The energy provided by the black hole is in most cases not significant for triggering the galactic wind. The observed high star-formation rates and metal overabundances are easily achieved, as are the constancy of chemical abundances with the redshift and present-day colours of bulges. Those results are not affected if we vary the index of the stellar IMF from $x = 0.95$ to $x = 1.35$. A steeper IMF is instead required in order to reproduce the colour-magnitude relation and the present K-band luminosity of the bulge.

Conclusions. We show that the chemical evolution of the host bulge, with a short formation timescale of ∼0.1 Gyr, a rather high efficiency of star formation ranging from 11 to 50 Gyr^{-1} according to the bulge mass, and an IMF flatter than the solar neighbourhood, combined with the accretion onto the black hole, is sufficient to explain the main observed features of Seyfert galaxies.

Key words. galaxies: Seyfert – galaxies: bulges – galaxies: photometry – ISM: abundances

1. Introduction

The outstanding question of the co-evolution of active galactic nuclei (AGN) and their host galaxies has received considerable attention in the past decades, since various pieces of evidence have pointed to a link between the formation of supermassive black holes (BHs) and the formation and evolution of their host spheroids: for example, the usual presence of massive dark objects at the centre of nearby spheroids (Ford et al. 1997; Ho 1999; Wandel 1999); the correlation between the BH mass and the stellar velocity dispersion of the host (for quiescent galaxies, Ferrarese & Merritt 2000; Gebhardt et al. 2000a; Tremaine et al. 2002; for active galaxies, Gebhardt et al. 2000b; Ferrarese et al. 2001; Shields et al. 2003; Onken et al. 2004; Nelson et al. 2004) or its mass (Kormendy & Richstone 1995; Magorrian et al. 1998; Marconi & Hunt 2003; Dunlop et al. 2003); the similarity between light evolution of quasar (QSO) population and the star formation history of galaxies (Cavaliere & Vittorini 1998; Haiman et al. 2004); the establishment of a good match among the optical QSO luminosity function, the luminosity function of star-forming galaxies and the mass function of dark matter halos (DMHs) at $z \sim 3$ (Haenhelt et al. 1998).

The most widely accepted explanation for the luminosity emitted by an AGNs is radiatively efficient gas accretion onto a central supermassive BH. The outflows from AGNs can profoundly affect the evolution of the host galaxy, e.g. by quenching or inducing the star formation (e.g., see Ciotti & Ostriker 2007, and references therein). The mutual feedback between galaxies and QSOs was used as a key to solving the shortcomings of the semianalytic models in galaxy evolution, e.g. the failure to account for the surface density of high-redshift massive galaxies (Blain et al. 2002; Cimatti et al. 2002) and for the α-enhancement as a function of mass (Thomas et al. 2002), since it could provide a way to invert the hierarchical scenario for the assembly of galaxies and star formation (see e.g. Monaco et al. 2000; Granato et al. 2004; Scannapieco et al. 2005).

The study of the chemical abundances of the QSOs was first undertaken by Hamann & Ferland (1993), who combined chemical evolution and spectral synthesis models to interpret the N V/C IV and N V/He II broad emission line ratios and found out that the high metallicities and the abundance ratios of the broad-line region are consistent with the outcomes of the models for giant elliptical galaxies (Arimoto & Yoshii 1987; Matteucci & Tornambè 1987; Angeletti & Giannone 1990), where the timescales of star formation and enrichment are very short and the initial mass function (IMF) is top-heavy. In the same year, Padovani & Matteucci (1993) and Matteucci & Padovani (1993) employed the chemical evolution model of Matteucci (1992)

to model the evolution of radio-loud QSOs, which are hosted by massive ellipticals, following in detail the evolution of several chemical species in the gas. They supposed that the mass loss from dying stars after the galactic wind provides the fuel for the central BH and modeled the bolometric luminosity as $L_{\rm bol} = \eta \dot{M} c^2$, with a typical value for the efficiency of $\eta = 0.1$, and were successful in obtaining the estimated QSO luminosities and the observed ratio of AGN to host galaxy luminosity. Then, they studied the evolution of the chemical composition of the gas lost by stars in elliptical galaxies and spiral bulges for various elements (C, N, O, Ne, Mg, Si, and Fe) and found out that the standard QSO emission lines were naturally explained by the high star-formation rate of spheroids at early times.

The relatively weak observed time dependence of the QSO abundances for $t \gtrsim 1$ Gyr was also predicted. The model of Matteucci & Padovani (1993) still followed the classic wind scenario, where the efficiency of star formation decreases with increasing galactic mass and which was found to be inconsistent with the correlation between spheroid mass and α-enhancement (Matteucci 1994). Moreover, Padovani & Matteucci (1993) pointed out that, if all mass lost by stars in the host galaxy after the wind were accreted by the central BH, the final BH mass would be up to two orders of magnitude higher than observed.

Other works (Friaça & Terlevich 1998; Romano et al. 2002; Granato et al. 2004), which had a more refined treatment of gas dynamics, limited their analysis of chemical abundances to the metallicity Z and the [Mg/Fe] ratio and their correlation with the galactic mass.

All these studies were mainly devoted to studying the coevolution of radio-loud QSOs and their host spheroids, which are elliptical galaxies. Now we want to extend the approach of Padovani & Matteucci (1993) to AGNs hosted by spiral bulges, with a more recent chemical evolution model for the bulge with the introduction of the treatment of feedback from the central BH and a more sophisticated way of dealing with the accretion rate. Since Seyfert nuclei tend to be hosted by disk-dominated galaxies (Adams 1977; Yee 1983; MacKenty 1990; Ho et al. 1997) our study can be applied to this class of objects.

The paper is organised as follows: in Sect. 2 we illustrate the chemical and photometrical evolution model, in Sect. 3 we show our calculations of the potential energy and of the feedback from supernovae (SNe) and from the AGN, in Sect. 4 we discuss our results concerning the black hole masses and luminosities, the chemical abundances, and the photometry, and in Sect. 5 we draw some conclusions.

2. The evolution model

2.1. Chemical evolution

The model on which we base our analysis is essentially the recent bulge chemical evolution model from Ballero et al. (2007a), which was successful in reproducing the most recent measurements of metallicity distribution (Zoccali et al. 2003; Fulbright et al. 2006) and evolution of abundance ratios (Origlia et al. 2002; Origlia & Rich 2004; Origlia et al. 2005; Rich & Origlia 2005; Fulbright et al. 2007; Zoccali et al. 2006; Lecureur et al. 2007) of the bulge giants. Here we summarise its main features.

- The gas is supposed to be well-mixed and homogeneous at any time (instantaneous mixing approximation).
- The star-formation rate (SFR) is parametrized as

$$\psi(r,t) \propto \nu \sigma^k_{\rm gas}(r,t). \quad (1)$$

In this expression, ν is the efficiency of star formation (a parameter whose meaning is that of the inverse of the timescale of star formation), $\sigma_{\rm gas}$ the gas surface mass density and k an index whose value can vary between 1 and 1.5 without giving rise to remarkable differences. We chose $k = 1$ to recover the star-formation law of spheroids. In our formalism the SFR is in units of $M_\odot\,{\rm Gyr}^{-1}\,{\rm pc}^{-2}$.

- The bulge forms by accreting gas from the Galactic halo at an exponential rate:

$$\dot{M}_{\rm inf} \propto {\rm e}^{-t/\tau}, \quad (2)$$

where τ is a suitable collapse timescale. The metallicity $Z_{\rm acc}$ of the accreted gas is approximately $\lesssim 10^{-4}\ Z_\odot$, but it is easily shown that the results are not significantly affected if we consider $Z_{\rm acc} = 0$.
- The type Ia SN rate is computed like in Matteucci & Recchi (2001) following the single degenerate scenario of Nomoto et al. (1984).
- Stellar lifetimes (Kodama 1997) are taken into account in detail. We adopted the stellar yields of François et al. (2004), which were constrained to reproduce the observed chemical abundances of the solar neighbourhood in the two-infall model of Chiappini et al. (2003).
- The adopted IMF is constant in space and time and has the shape of a multi-part power law:

$$\phi(M) \propto M^{-(1+x_i)} \quad (3)$$

where the subscript refers to different mass ranges. Its normalization is performed by assuming a stellar mass range of $0.1{-}80\ M_\odot$.

In the reference model of Ballero et al. (2007a), the parameters that allow a best fit of the metallicity distributions and the [α/Fe] vs. [Fe/H] ratios measured in the bulge giants are the following: $\nu = 20\ {\rm Gyr}^{-1}$, $\tau = 0.1$ Gyr, and two slopes for the IMF, namely $x_1 = 0.33$ for $0.1 \le M/M_\odot \le 1$ (in agreement with the photometric measurements of Zoccali et al. 2000) and $x_2 = 0.95$ for $1 \le M/M_\odot \le 80$. We also considered the case $x_2 = 1.35$ (Salpeter 1955) for comparison.

This model holds for a galaxy like ours with a bulge of $M_{\rm b} = 2 \times 10^{10}\ M_\odot$. We are going to predict the properties of Seyfert nuclei hosted by bulges of different masses, therefore some model parameters will have to be re-scaled. We choose to keep the IMF constant and to scale the effective radius and the star formation efficiency following the inverse-wind scenario (Matteucci 1994). The possibility of changing the infall timescale with mass is not explored in the present paper. Table 1 reports the adopted parameters for each bulge mass.

Table 1. Features of the examined models: in order, bulge mass, star formation efficiency, bulge effective radius. The table also reports the time of occurrence of the galactic wind.

$M_{\rm b}$ ($M_\odot$)	ν (Gyr^{-1})	$R_{\rm e}$ (kpc)	$t_{\rm GW}$ (Gyr)
2×10^9	11	1	0.31
2×10^{10}	20	2	0.27
10^{11}	50	4	0.22

2.2. The spectro-photometric model

By matching chemical evolution models with a spectro-photometric code, it has been possible to reproduce the present-day photometric features of galaxies of various morphological

types (Calura & Matteucci 2006; Calura et al. 2007a) and to perform detailed studies of the evolution of the luminous matter in the Universe (Calura & Matteucci 2003; Calura et al. 2004). By means of the chemical evolution model plus a spectro-photometric code, we attempt here to model the photometric features of galactic bulges. All the spectro-photometric calculations are performed by means of the code developed by Jimenez et al. (2004), and based on new stellar isochrones computed by Jimenez et al. (1998) and on the stellar atmospheric models by Kurucz (1992). The main advantage of this photometric code is that it allows us to follow in detail the metallicity evolution of the gas, thanks to the large number of simple stellar populations calculated by Jimenez et al. (2004) by means of new stellar tracks, with ages between 1×10^6 and 1.4×10^{10} yr and metallicities ranging from $Z = 0.0002$ to $Z = 0.1$.

Starting from the stellar spectra, we first build simple stellar population (SSP) models consistent with the chemical evolution at any given time and weighted according to the assumed IMF. Then, a composite stellar population (CSP) consists of the sum of different SSPs formed at different times, with a luminosity at an age t_0 and at a particular wavelength λ given by

$$L_\lambda(t_0) = \int_0^{t_0} \int_{Z_\mathrm{i}}^{Z_\mathrm{f}} \psi(t_0 - t) L_{\mathrm{SSP},\lambda}(Z, t_0 - t) \mathrm{d}Z \mathrm{d}t, \quad (4)$$

where the luminosity of the SSP can be written as

$$L_{\mathrm{SSP},\lambda}(Z, t_0 - t) = \int_{M_\mathrm{min}}^{M_\mathrm{max}} \phi(M) l_\lambda(Z, M, t_0 - t) \mathrm{d}M \quad (5)$$

and where $l_\lambda(Z, M, t_0 - t)$ is the luminosity of a star of mass M, metallicity Z, and age $t_0 - t$; Z_i and Z_f are the initial and final metallicities, M_min and M_max are the lowest and highest stellar masses in the population, $\phi(M)$ is the IMF, and $\psi(t)$ is the SFR at the time t. Peletier et al. (1999) have shown that dust in local bulges is very patchy and concentrated in the innermost regions, i.e. within distances of ∼100 pc. They also show that dust extinction effects are negligible at distances of $\sim 1\ R_\mathrm{eff}$. In addition, we compared our photometric predictions to observational results largely unaffected by dust, such as the ones by Balcells & Peletier (1994). For these reasons, in all our spectro-photometric calculations, we do not take dust extinction into account.

3. Energetics and AGN feedback

The bulge lies in the potential well of the Galaxy, which consists of both luminous and dark matter. In the model of Ballero et al. (2007a), we calculated the binding energy ΔE_g of the bulge gas following Bertin et al. (1992), i.e. by treating the bulge as a scaled-down two-component elliptical (thus ignoring the disk contribution). We also assumed that the thermal energy of the bulge interstellar medium was mainly contributed by the explosion of type I and type II supernovae. In particular, if we call E_th the gas thermal energy, we supposed that at time t_GW, when the condition

$$E_\mathrm{th}(t_\mathrm{GW}) = \Delta E_\mathrm{g}(t_\mathrm{GW}) \quad (6)$$

is satisfied, a wind develops and the star formation is suppressed. In the reference model of Ballero et al. (2007a), this event does not have a strong impact on the predicted chemical evolution, since it occurs when most of the gas has already been processed into stars. However, the high-metallicity tail of the metallicity distribution was somewhat overestimated without the galactic wind.

In the present exploration, not only do we adopt a more realistic disk galaxy model to better estimate the binding energy of the gas in the bulge, but we also consider the additional contribution to the gas thermal energy given by the BH feedback, so that

$$E_\mathrm{th}(t) = E_{\mathrm{th,SN}}(t) + E_{\mathrm{th,AGN}}(t). \quad (7)$$

The various simplifying assumptions adopted in the evaluation of the gas binding energy and of the BH feedback will be discussed in some detail in the following sections.

3.1. The gas binding energy

If we define

$$\Psi(r, t) = \pi R_\mathrm{e}^2 \psi(r, t) \quad (8)$$

and

$$\dot{M}_* = \int_{0.1}^{80} \phi(M) \Psi(r, t - \tau_M) R_M(t - \tau_M) \mathrm{d}M \quad (9)$$

where R_M is the return mass fraction (i.e. the fraction of mass in a stellar generation that is ejected into the interstellar medium by stars of mass M; see Tinsley 1980) and τ_M is the lifetime of a star of mass M, then, before the galactic wind, the mass of gas in the bulge evolves at a rate

$$\dot{M}_\mathrm{g}(t < t_\mathrm{GW}) = \dot{M}_\mathrm{inf} + \dot{M}_* - \Psi(r, t) - \dot{M}_\mathrm{BH}; \quad (10)$$

i.e. gas is accreted from the halo, is restituted by stellar mass loss, and is subtracted by star formation and black hole accretion. After the wind, star formation vanishes and we suppose that, the infall is arrested due to the development of a global outflow. Therefore, this equation reduces to

$$\dot{M}_\mathrm{g}(t > t_\mathrm{GW}) = \dot{M}_* - \dot{M}_\mathrm{BH} - \dot{M}_\mathrm{W} \quad (11)$$

where $\dot{M}_\mathrm{W}$ is the rate of mass loss due to the galactic wind. We assume that all the gas present at a given time is lost, so that $\dot{M}_\mathrm{W} = \dot{M}_* - \dot{M}_\mathrm{BH}$. In the present treatment the galaxy mass model is required in order to estimate the binding energy of the gas in the bulge, a key ingredient in establishing the wind phase. In particular, the current galaxy model is made by three different components, namely:

– A spherical Hernquist (1990) distribution representing the stellar component of the bulge:

$$\begin{cases} \rho_\mathrm{b}(r) &= \dfrac{M_\mathrm{b}}{2\pi} \dfrac{r_\mathrm{b}}{r(r + r_\mathrm{b})^3}, \\ \Phi_\mathrm{b}(r) &= -\dfrac{GM_\mathrm{b}}{r + r_\mathrm{b}}, \end{cases} \quad (12)$$

where M_b is the bulge mass, Φ_b the bulge potential and r_b the scale radius of the bulge, related to its effective radius by $R_\mathrm{e} \simeq 1.8 r_\mathrm{b}$.

– A spherical isothermal dark matter halo with circular velocity v_c:

$$\begin{cases} \rho_\mathrm{DM}(r) &= \dfrac{v_\mathrm{c}^2}{4\pi G r^2} \\ \Phi_\mathrm{DM}(r) &= v_\mathrm{c}^2 \ln \dfrac{r}{r_0} \end{cases} \quad (13)$$

where r_0 is an arbitrary scale-length.

– A razor-thin exponential disk with surface density

$$\Sigma_{\rm d}(R) = \frac{M_{\rm d}}{2\pi R_{\rm d}^2} {\rm e}^{-R/R_{\rm d}}, \quad (14)$$

where $M_{\rm d}$ is the total disk mass, R the cylindrical radius, and $R_{\rm d}$ the disk scale radius. As is well known, the gravitational potential of a disk can in general be expressed by using the Hankel-Fourier transforms (e.g., Binney & Tremaine 1987): however, as shown in Appendix A, under the assumption of a spherical gas distribution, the contribution to the gas binding energy can be easily calculated without using the explicit disk potential.

In fact, we assume that the gas distribution before the establishment of the galactic wind is spherically symmetric and parallel to the stellar one; i.e.

$$\rho_{\rm g}(r) = \frac{M_{\rm g}}{2\pi} \frac{r_{\rm b}}{r(r+r_{\rm b})^3}. \quad (15)$$

In order to estimate the energy required to induce a bulge wind, we define a *displacement radius* $r_{\rm t}$, and we calculate the energy required to displace at $r_{\rm t}$ the gas contained at $r < r_{\rm t}$ (while maintaining spherical symmetry). We adopt a fiducial value of $r_{\rm t} = 3R_{\rm e}$; the calculated values of the binding energy do not change significantly for $r_{\rm t}$ ranging from $2R_{\rm e}$ to $10R_{\rm e}$. A spherically symmetric displacement (while not fully justified theoretically) allows a simple evaluation of the gas binding energy, and it is acceptable in the present approach. Consistent with the assumption above,

$$\Delta E_{\rm g} = \Delta E_{\rm gb} + \Delta E_{\rm gDM} + \Delta E_{\rm gd}, \quad (16)$$

where the various terms at the r.h.s. describe the gas-to-bulge, gas-to-DM, and gas-to-disk contributions. Elementary integrations show that

$$\begin{aligned} \Delta E_{\rm gb} &= 4\pi \int_0^{r_{\rm t}} \rho_{\rm g}(r)[\Phi_{\rm b}(r_{\rm t}) - \Phi_{\rm b}(r)] r^2 {\rm d}r \\ &= \frac{G M_{\rm g} M_{\rm b}}{r_{\rm b}} \frac{\delta^3}{3(1+\delta)^3}, \end{aligned} \quad (17)$$

and

$$\begin{aligned} \Delta E_{\rm gDM} &= 4\pi \int_0^{r_{\rm t}} \rho_{\rm g}(r)[\Phi_{\rm DM}(r_{\rm t}) - \Phi_{\rm DM}(r)] r^2 {\rm d}r \\ &= M_{\rm g} v_{\rm c}^2 \left[\ln(1+\delta) - \frac{\delta}{1+\delta} \right], \end{aligned} \quad (18)$$

where $\delta \equiv r_{\rm t}/r_{\rm b}$, while

$$\Delta E_{\rm gd} = \frac{G M_{\rm g} M_{\rm d}}{R_{\rm d}} \times \widetilde{\Delta E_{\rm gd}}, \quad (19)$$

and the function $\widetilde{\Delta E_{\rm gd}}$ is given in Appendix. Of course, $\Delta E_{\rm g}$ is linearly proportional to the gas mass in the bulge.

In Fig. 1 we see that, for a $10^{10}\ M_\odot$ bulge like ours, the dominant contribution arises from the dark matter halo, whereas the bulge and disk contributions are comparable, both about one order of magnitude smaller than the dark matter halo one. This differs from previous calculations (Ballero et al. 2007a) in the way that the bulge contribution is reduced by almost one order of magnitude. The same is true for the bulges of other masses. We must consider, moreover, that in the inside-out scenario for Galactic formation (Chiappini et al. 1997) the disk will probably form much later than the bulge, so its contribution to the potential well during the bulge formation could be negligible. Thus, what we explore is the extreme hypothesis that the disk has been in place since the beginning.

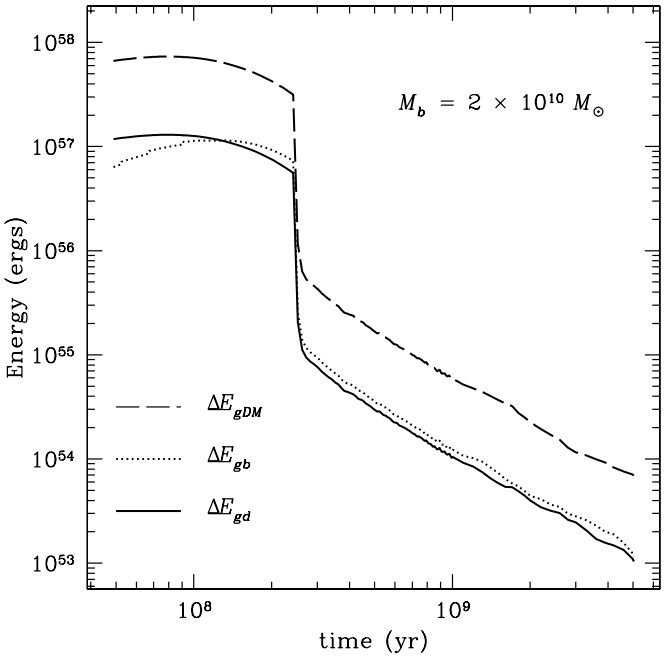

Fig. 1. Time evolution of the different contributions to the gas binding energy in the bulge of a Milky Way like galaxy: dark matter halo (dashed line), bulge (dotted line), and exponential disk (solid line). In particular, $M_{\rm b} = 2 \times 10^{10}\ M_\odot$, $R_{\rm e} = 2$ kpc, $v_{\rm c} = 200$ km s^{-1}, $M_{\rm d} = 10^{11}\ M_\odot$, and $R_{\rm d} = 4.3$ kpc.

3.2. Feedback from supernovae

The cumulative thermal energy injected by SNe is calculated as in Pipino et al. (2002). Namely, if we call $R_{\rm SNIa/II}(t)$ the rate of type Ia/II SN explosions, then

$$E_{\rm th,SN}(t) = E_{\rm th,SNIa}(t) + E_{\rm th,SNII}(t), \quad (20)$$

where

$$E_{\rm th,SNIa/II}(t) = \int_0^t \epsilon(t-t') R_{\rm SNIa/II}(t') {\rm d}t' {\rm erg}. \quad (21)$$

The evolution with time of the thermal content ϵ of an SN remnant, needed in the equation above, is given by (Cox 1972):

$$\epsilon(t_{\rm SN}) = \begin{cases} 7.2 \times 10^{50} \epsilon_0 & {\rm erg\ \ for\ \ } 0 \le t_{\rm SN} \le t_{\rm c}, \\ 2.2 \times 10^{50} \epsilon_0 (t_{\rm SN}/t_{\rm c})^{-0.62} & {\rm erg\ \ for\ \ } t_{\rm SN} \ge t_{\rm c}, \end{cases} \quad (22)$$

where ϵ_0 is the initial blast wave energy of an SN in units of 10^{51} erg, assumed equal for all SN types, $t_{\rm SN}$ is the time elapsed since explosion, and $t_{\rm c}$ is the metallicity-dependent cooling time of an SN remnant (Cioffi et al. 1988):

$$t_{\rm c} = 1.49 \times 10^4 \epsilon_0^{3/14} n_0^{-4/7} \zeta^{-5/14}\ {\rm yr}. \quad (23)$$

In this expression $\zeta = Z/Z_\odot$, and n_0 is the hydrogen number density.

3.3. Accretion onto and feedback from the central black hole

In our phenomenological treatment of BH feedback, we only considered radiative feedback, thus neglecting other feedback mechanisms such as radiation pressure and relativistic particles, as well as the mechanical phenomena associated with jets. From this point of view we are following the approach described in

Sazonov et al. (2005), even though several aspects of the physics considered there (in the context of elliptical galaxy formation) are not taken into account. In fact, we note that these phenomena can only be treated in the proper way by using hydrodynamical simulations.

We suppose that the bulge gas is fed into the spherically accreting BH at the Bondi rate $\dot{M}_{\rm B}$. However, the amount of accreting material cannot exceed the Eddington limit, i.e.

$$\dot{M}_{\rm BH} = \min(\dot{M}_{\rm Edd}, \dot{M}_{\rm B}). \tag{24}$$

The Eddington accretion rate, i.e. the accretion rate beyond which radiation pressure overwhelms gravity, is given by

$$\dot{M}_{\rm Edd} = \frac{L_{\rm Edd}}{\eta c^2} \tag{25}$$

where η is the efficiency mass-to-energy conversion. In general, $0.001 \leq \eta \leq 0.1$, and we adopt the maximum value $\eta = 0.1$ (Yu & Tremaine 2002). The Eddington luminosity is given by

$$L_{\rm Edd} = 1.3 \times 10^{46} \frac{M_{\rm BH}}{10^8\ M_\odot}\ \ {\rm erg\ s^{-1}}. \tag{26}$$

The Bondi accretion rate describes the stationary flow of gas from large distances onto the black hole, for a given gas temperature and density (see Bondi 1952), and is given by

$$\dot{M}_{\rm B} = 4\pi R_{\rm B}^2 \rho_{\rm B} c_{\rm S}, \tag{27}$$

where

$$R_{\rm B} = \frac{GM_{\rm BH}\mu m_{\rm p}}{2\gamma kT} = 16\ \ {\rm pc}\ \frac{1}{\gamma}\frac{M_{\rm BH}}{10^8\ M_\odot}\left(\frac{T}{10^6\ {\rm K}}\right)^{-1} \tag{28}$$

with

$$c_{\rm s}^2 = \left(\frac{\partial p}{\partial \rho}\right)_{\rm isot} = \frac{kT}{\mu m_{\rm p}}, \tag{29}$$

and $\rho_{\rm B}$ (the gas density at $R_{\rm B}$) can be estimated as

$$\rho_{\rm B} = \frac{\bar{\rho}_{\rm e}}{3}\left(\frac{R_{\rm e}}{R_{\rm B}}\right)^2. \tag{30}$$

In the code we adopt $\gamma = 1$ (isothermal flow). If we assume that all the gas mass is contained within 2 $R_{\rm e}$, the mean gas density within $R_{\rm e}$ is given by

$$\bar{\rho}_{\rm e} = \frac{3M_{\rm g}}{8\pi R_{\rm e}^3}. \tag{31}$$

The equilibrium gas temperature can be estimated as the bulge virial temperature,

$$T_{\rm vir} \simeq \frac{\mu m_{\rm p}\sigma^2}{k} = 3.0 \times 10^6\ {\rm K}\left(\frac{\sigma}{200\ {\rm km\ s^{-1}}}\right)^2, \tag{32}$$

where σ is the one-dimensional stellar velocity dispersion in the bulge, which is given by

$$\sigma^2 \equiv -\frac{W_{\rm b}}{3M_{\rm b}}. \tag{33}$$

The virial potential trace $W_{\rm b}$ for the bulge is obtained by summing the contribution of the three galaxy components, i.e.

$$\begin{aligned} W_{\rm b} &= W_{\rm bb} + W_{\rm bDM} + W_{\rm bd} \\ &= -\frac{GM_{\rm b}^2}{6r_{\rm b}} - M_{\rm b}v_{\rm c}^2 - \frac{GM_{\rm d}M_{\rm b}\widetilde{W_{\rm bd}}}{R_{\rm d}} \end{aligned} \tag{34}$$

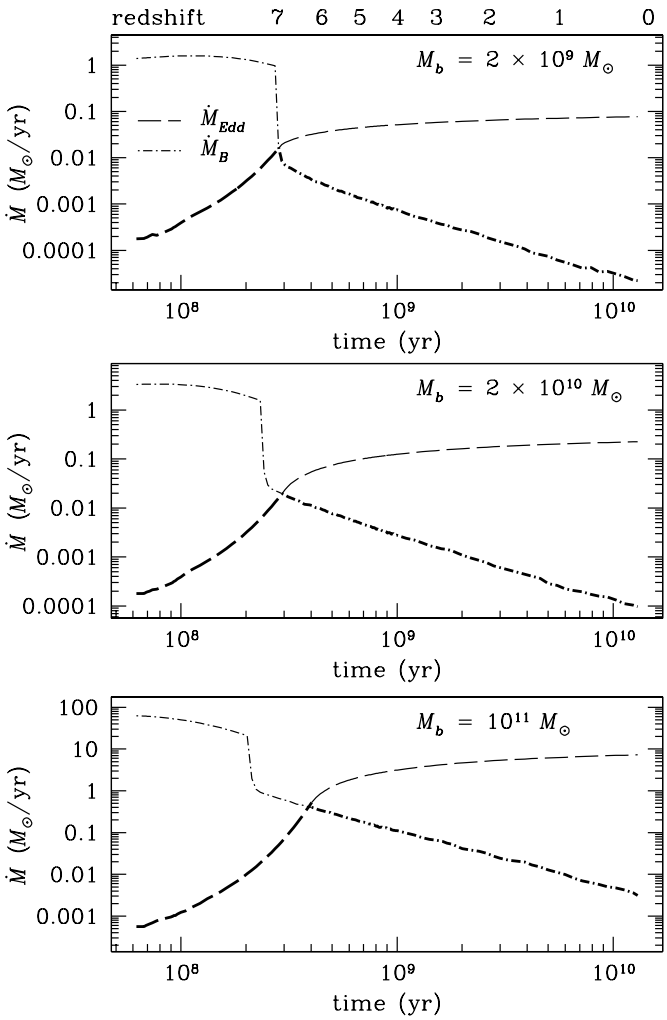

Fig. 2. Time evolution of the Eddington (dashed line) and Bondi (dot-dashed line) accretion rates for bulges with various masses. The thicker lines indicate the resulting accretion rate, which is assumed to be the minimum between the two.

where the term $\widetilde{W_{\rm bd}}$ is given in Appendix. The bolometric luminosity emitted by the accreting BH is then calculated as

$$L_{\rm bol} = \eta c^2 \dot{M}_{\rm BH}. \tag{35}$$

Finally, we assume that the energy released by the black hole is the integral of a fraction f of this luminosity over the time-step:

$$E_{\rm th,BH} = f\int_t^{t+\Delta t} L_{\rm bol}{\rm d}t \simeq f L_{\rm bol}\Delta t. \tag{36}$$

The value of f can vary between 0 and 1; we assume $f = 0.05$ (Di Matteo et al. 2005). The seed black hole mass was modified in a range 5×10^2–$5 \times 10^4\ M_\odot$ without any appreciable change in the results. Therefore, we adopted a universal seed black hole mass of $10^3\ M_\odot$.

4. Results

4.1. Mass loss and energetics

Figure 2 shows the evolution of the Eddington and Bondi accretion rates with time and redshift. The redshift was calculated assuming a ΛCDM cosmology with $H_0 = 65\ {\rm km\,s^{-1}\,Mpc^{-1}}$,

$\Omega_M = 0.3$, and $\Omega_\Lambda = 0.7$, and a redshift of formation of $z_f \simeq 10$. We can see that the history of accretion onto the central BH can be divided into two phases: the first, Eddington-limited, and the second, Bondi-limited. Most of the accretion and fueling occurs around the period of transition between the two phases, which coincides approximately with the occurrence of the wind although it extends for some time further in the most massive models. The details of the transition depend on the numerical treatment of the wind, however since the gas consumption in the bulge is very fast, and the Bondi rate depends on the gas density, we can expect that the results would not change significantly even if we modeled the galactic wind as a continuous wind. The BH mass is essentially accreted, within a factor of two, in a period ranging from 0.3 to 0.8 Gyr, i.e. 2 to 6% of the bulge lifetime, which we assume to be 13.7 Gyr.

Figure 3 compares the different contributions to the thermal energy, i.e. the feedback from SNe and from the AGN, with the potential energy. We see that only in the case of $M_b = 2\times10^9\ M_\odot$ does the BH feedback provide a thermal energy comparable to what is produced by the SN explosions before the onset of the wind[1]. Therefore, in the context of chemical and photometrical evolution, the contribution of the BH feedback is negligible in most cases, unless we assume an unrealistically large fraction of the BH luminosity is transferred to the ISM. Note that this conclusion is also supported by hydrodynamical simulations specifically designed to study the effects of radiative BH feedback in elliptical galaxies (Ciotti & Ostriker 1997, 2001, 2007; Ostriker & Ciotti 2005). Also, Di Matteo et al. (2003) showed that it is unlikely that black hole accretion plays a crucial role in the general process of galaxy formation, unless there is strong energetic feedback by active QSOs (e.g. in the form of radio jets).

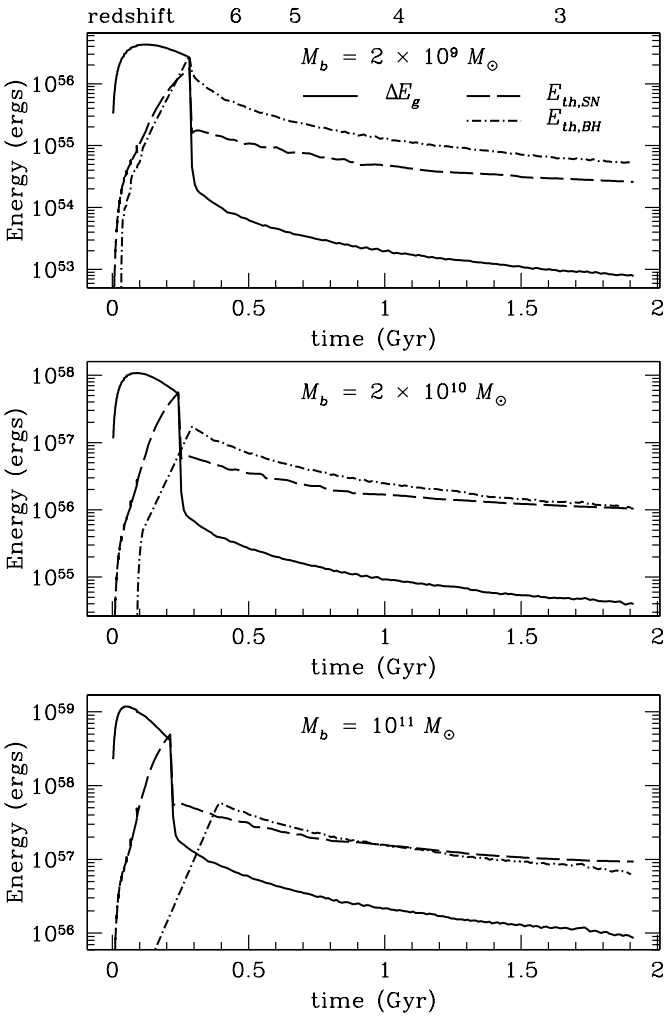

Fig. 3. Energy balance as a function of time for bulges with various masses. The figure shows the gas binding energy (solid line) compared to the thermal energy released by supernovae (dashed line) and the accreting black hole (dot-dashed line).

4.2. Star-formation rate

Figure 4 shows the evolution of the global SFR in the bulge as a function of time and redshift. The break corresponds to the occurrence of the galactic wind. It is evident that, in the case of the most massive bulges, it is easy to reach the very high SFRs of a few times 1000 $M_\odot$/yr inferred from observations at high redshifts (e.g. Maiolino et al. 2005). It is worth noting that this result matches the statement of Nagao et al. (2006) very well, that the absence of a significant metallicity variation up to $z \simeq 4.5$ implies that the active star-formation epoch of QSO host galaxies occurred at $z \gtrsim 7$. There is evidence of some tiny downsizing (star formation ceases at slightly earlier times for larger galaxies; see Table 1). We stress that we are making predictions about single galaxies and not about the AGN population, and we only want to show that it is possible to achieve such high rates of star formation in a few Myrs.

4.3. Black hole masses and luminosities

In Fig. 5 we show the final BH masses resulting from the accretion as a function of the bulge mass. The predicted BH masses, which are reached in a few hundred Myrs, are in good agreement with measurements of BH masses inside Seyfert galaxies (Wandel et al. 1999; Kaspi et al. 2000; Peterson 2003). This is a valuable result, given the simplistic assumptions of our model, since in this case we did not have to stop accretion in an artificial way as in Padovani & Matteucci (1993); in fact, the BH growth at late times is limited by the available amount of gas, as described by Bondi accretion. The figure suggests an approximately linear relation between the bulge and BH mass, as first measured by Kormendy & Richstone (1995) and Magorrian et al. (1998). Therefore, Seyfert galaxies appear to obey the same relationship as quiescent galaxies and QSOs, as already stated observationally by Nelson et al. (2004).

There were claims for a non-linear relation between spheroid and black hole mass (Laor 2001; Wu & Han 2001); however, measurements of Marconi & Hunt (2003) re-established the direct proportionality between the spheroid mass M_{sph} and M_{BH},

$$M_{BH} \simeq 0.0022\ M_{sph}, \tag{37}$$

also in good agreement with recent estimates from McLure & Dunlop (2002) and Dunlop et al. (2003)

$$M_{BH} \simeq 0.0012\ M_{sph} \tag{38}$$

and from Häring & Rix (2004)

$$M_{BH} \simeq 0.0016\ M_{sph}. \tag{39}$$

The three relations of McLure & Dunlop (2002), Marconi & Hunt (2003), and Häring & Rix (2004) are thus reported in the

[1] The Bondi accretion rate does not vanish even if the thermal energy of the ISM is greater than the potential energy, due to the fresh gas provided by the stellar mass losses of the aging stars in the bulge.

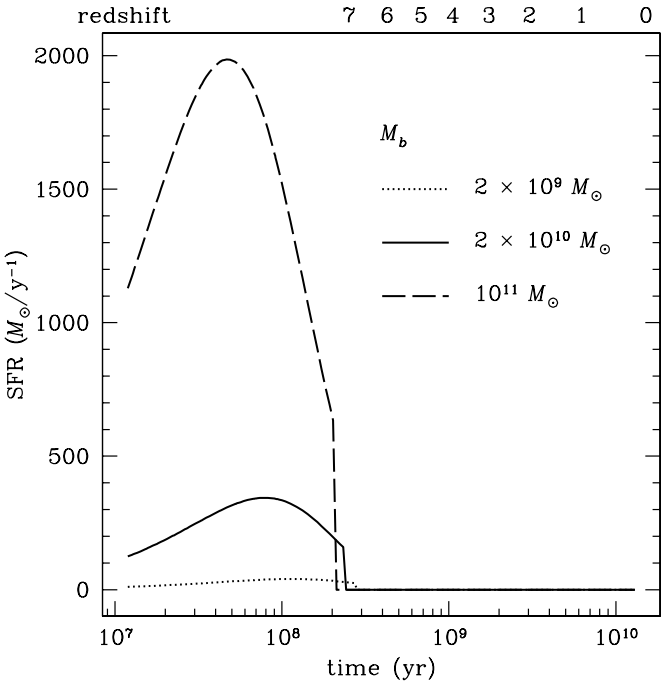

Fig. 4. Star formation rate as a function of time and redshift for bulges with various masses. The peak value of the $M_b = 2 \times 10^9\ M_\odot$ case is ~40 $M_\odot$/yr.

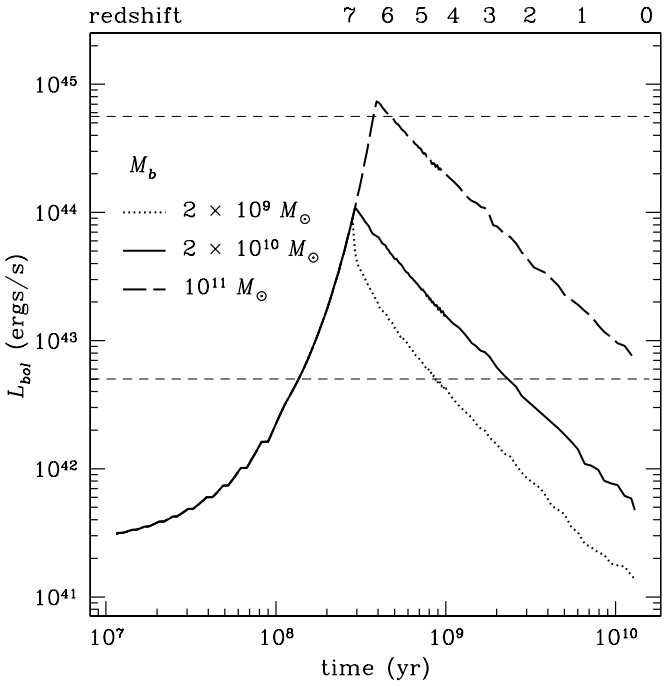

Fig. 6. Evolution with time and redshift of the bolometric luminosity emitted by the accreting BH for bulges of various masses. The dotted lines represent the range spanned by observations (see text for details).

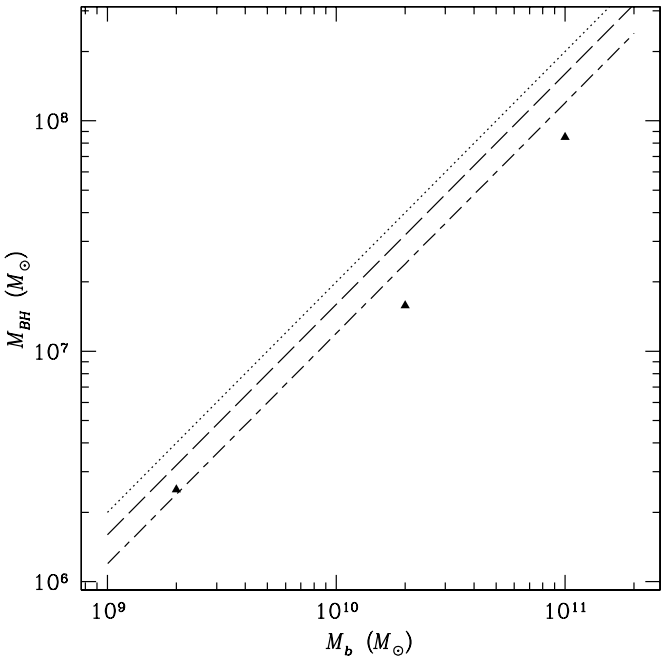

Fig. 5. Final black-hole masses as a function of the bulge mass predicted by our models (triangles). The short dashed-long dashed line represents the measured relation of McLure & Dunlop (2002), the dotted line the one of Marconi & Hunt (2003), and the dashed line the one of Häring & Rix (2004).

figure for comparison. The agreement between measurements and predictions is rather good (within a factor of two).

In Fig. 6 we plot the predicted bolometric nuclear luminosities $L_{\rm bol}$ for the various masses, compared with luminosity estimates for the Seyfert population (see e.g. González Delgado et al. 1998; Markowitz et al. 2003; Brandt & Hasinger 2005; Wang & Wu 2005; Gu et al. 2006). Of course, $L_{\rm bol}$ is proportional to the calculated mass accretion rate (Fig. 2). In the first part, the plots overlap because the Eddington luminosity only depends on the BH mass, and it is independent of the galaxy mass; on the contrary, the Bondi accretion rate is sensitive to the galaxy features. The break in the plot corresponds to the time when the Bondi accretion rate becomes smaller than the Eddington accretion rate (see Eqs. (25) and (27)), and the break occurs later and later for more massive galaxies, which therefore keep accreting at the Eddington rate on longer timescales. This helps explain why the outcoming final black hole mass is proportional to the adopted bulge mass.

We see that the luminosities near the maximum are reproduced by models of all masses. The same is not true for local ($z \simeq 0$) Seyferts, because only the most massive model yields a bolometric luminosity that lies in the observed range, while for other masses, the disagreement reaches a factor of ~100. To simply shift the epoch of star formation of the less massive Seyferts would require unrealistically young bulges ($\lesssim$1 Gyr), whereas one of our main assumptions is that spiral bulges are old systems. Padovani & Matteucci (1993) assumed that the BH accreted the whole mass lost from evolved stars. If we calculate the fraction $\dot{M}_{\rm B}/\dot{M}_*$ at any given time, we see that its value is very close to 0.01. This explains why they obtained the correct nuclear bolometric luminosity of local radio-loud QSOs, but severely overestimated the mass of the resulting BH, which led them to suggest that the accretion phase should last for a period not longer than a few 10^8 years, at variance with the present work. Moreover, it is not physically justified to assume that all the mass expelled from dying stars falls onto the black hole.

One way to overcome this problem is to suppose that the smallest bulges undergo a rejuvenation phase, which is possible because spiral bulges are not isolated systems, but an interaction with their surrounding disks can be triggered in several

ways (bar instabilities, minor mergers, fly-bys, and so on). Using models combining recent star formation with a base old population, Thomas & Davies (2006) found that the smallest bulges must have experienced star formation events involving 10−30% of their total mass in the past 1−2 Gyr. The same conclusion was also reached on an independent basis by MacArthur et al. (2007), who studied a sample of 137 spiral bulges in the GOODS fields and, by means of photometric techniques, estimated the star formation necessary to reproduce the observed color range. They concluded that, while all stellar populations belonging to bulges with $M_B > 10^{11}\ M_\odot$ are homogeneously old and consistent with a single major burst of star formation at $z > 2$, the colors and mass-to-light ratios of smaller bulges require that they have experienced mass growth since $z \sim 1$, so that a ∼10% fraction of stellar mass eventually goes into younger stars.

Secondary accretion/star formation episodes may also help explain the presence of the Galactic bulge Mira population, whose calculated age is 1−3 Gyr (van Loon et al. 2003; Groenewegen & Blommaert 2005) and of young star and star clusters in the very centre of the Galaxy (Figer et al. 1999; Genzel et al. 2003). A small fraction of intermediate-age stellar population was also detected in Seyfert 2 nuclei (Sarzi et al. 2007).

Finally, we note that, by means of the present (non-hydrodynamical) modeling of the BH accretion rate and of the gas budget, a truly realistic accretion cannot be reproduced, whereas in a more realistic treatment, the AGN feedback would cause the luminosity to switch on and off several times at the peaks of luminosity. We also note that at late times, when the accretion is significantly sub-Eddington, a considerable reduction in the emitted AGN luminosity might result as a consequence of a possible radiatively inefficient accretion mode (e.g., Narayan & Yi 1994). This could reproduce the quiescence of black holes at the centre of present-day inactive spiral galaxies.

4.4. Chemical abundances and metallicities

Observations of QSOs and Seyferts

Estimates of chemical abundance ratios in AGNs are not an easy task. The use of emission lines is subject to large uncertainties due to the dependence of the lines on several parameters that are difficult to quantify (e.g. column density, microtubulence, collisional excitation, etc.). This is a problem since most measurements of the [Fe/Mg] abundance ratio, which provides a clock for constraining the ages of QSOs and their timescales of enrichment, rely on the flux ratio of the Fe II (UV bump) and Mg II (λ2800) emission lines. The true physical origin of the Fe II UV complex was questioned by Verner et al. (2003), Baldwin et al. (2004), and Korista et al. (2004), who show that the flux ratio does not scale directly with the abundance ratio due to the thermostatic effect of coolants. Absorption lines could be a better probe of QSO environments, especially narrow absorption lines that avoid saturation and blending of important abundance diagnostics. However, these data require large signal-to-noise ratios and are therefore harder to obtain. Moreover, they are not free from uncertainties concerning the shape of ionizing spectrum, the lack of ionization constraints, the unknown coverage fraction, and the exact location of the absorbers (see Hamann & Ferland 1999 for an extensive review about QSO abundance diagnostics).

Given these caveats, it is evident, in any case, that the emission spectrum of AGNs is particularly similar for a very wide range of redshifts and luminosities (Osmer & Shields 1999). The most probable explanation is a similarity of chemical abundances. In particular, the analysis of the Fe II(UV bump)/Mg II(λ2800) flux ratio in various redshift ranges (Thompson et al. 1999; Iwamuro et al. 2002; Freudling et al. 2003; Dietrich et al. 2003a; Barth et al. 2003; Maiolino et al. 2003; Iwamoto et al. 2004) is consistent with an [Fe/Mg] abundance ratio that is slightly supersolar and almost constant for redshifts out to $z \sim 6.4$. This result was also confirmed for $z \sim 6$ QSOs by very recent works (Kurk et al. 2007; Jiang et al. 2007). A weak trend with luminosity has been detected (Dietrich et al. 2003a).

Due to the time delay necessary for Fe enrichment from type Ia SNe in a star formation history typical of elliptical galaxies (see Matteucci & Recchi 2001), this means that the surrounding stellar population must already be in place by the time the AGN shines and that, in a well-mixed ISM, star formation must have begun $\gtrsim 10^8$ years before the observed activity, i.e. at redshifts $z_f \gtrsim 10$ (Hamann et al. 2002; Hamann et al. 2004).

Many efforts have been devoted to the measurement of nitrogen lines, since due to its secondary nature[2], the N abundance relative to its seed nuclei (e.g. oxygen) is a good proxy for metallicity. As abundance indicators, broad emission line ratios of N V/C IV and N V/He II were analysed by Hamann & Ferland (1993). Hamann & Ferland (1999) also indicated N V/C IV and N V/O VI in narrow absorption line systems as possible abundance indicators. Hamann et al. (2002) instead favour N III]/O III] and N V/(C IV + O VI) as the most robust abundance indicators. The general conclusions drawn from these diagnostics are that the AGNs appear to be metal rich at all observed redshifts, with metallicities ranging from solar up to ∼10 times solar. Dietrich et al. (2003b) studied a sample of 70 high-redshift QSOs ($3.5 \lesssim z \lesssim 5.0$) and, based on emission-line flux ratios involving C, N, O and He, estimated an average overall metallicity of ∼4−5 $Z_\odot$ for the emitting gas. A similar estimate (∼5 $Z_\odot$) was drawn more recently by Nagao et al. (2006), who examined 5344 spectra of high-redshift ($z \geq 2$) QSOs taken from the SDSS DR2; they also confirm the detected trend in the N/He and N/C emission line ratios, which suggests that there might be a correlation with luminosity, i.e. more luminous QSOs, residing in more massive galaxies, are more metal rich. Bentz et al. (2004) suggested that some very nitrogen-enriched QSOs could be viewed at the peak of metal enrichment, e.g. near the end of their accretion phases, although their conclusions are not definite. Work carried out on intrinsic narrow absorption line systems (Petitjean & Srianand 1999; Hamann et al. 2003; D'Odorico et al. 2004) confirms that the observed N, C, and Si abundance ratios are consistent with at least solar metallicities. In particular, D'Odorico et al. (2004) interpreted their observations as suggestive of a scenario of rapid enrichment due to a short (∼1 Gyr) star formation burst. The amount of emission from dust and CO in high-redshift QSOs (Cox et al. 2002) corroborate the idea of massive amounts of star formation preceding the shining of the AGN. However, there is no need for exotic scenarios to explain the production of heavy elements near QSOs (e.g. central star clusters, star formation inside accretion disks), since normal chemical evolution of ellipticals is sufficient to this purpose (Hamann & Ferland 1993; Matteucci & Padovani 1993).

The majority of conclusions concerning QSOs has been found to hold also for Seyfert galaxies, i.e. observations seem

[2] We recall that an element is secondary when it is produced starting from a seed non-primordial nucleus; therefore, its abundance is very sensitive on the metallicity of the gas where it is formed.

to confirm that most Seyfert galaxies are metal rich. An overabundance of nitrogen by a factor ranging from about 2 to 5 was first detected in the narrow line region of Seyferts by Storchi-Bergmann & Pastoriza (1989, 1990), Storchi-Bergmann et al. (1990), and Storchi-Bergmann (1991), and was later confirmed by Schmitt et al. (1994). Further work by Storchi-Bergmann et al. (1996) allowed them to derive the chemical composition of the circumnuclear gas in 11 AGNs, and high metallicities were found (O ranging from solar to 2−3 times solar and N up to 4−5 times solar). This trend was also measured in more recent works (Wills et al. 2000; Mathur 2000). Fraquelli & Storchi-Bergmann (2003) examined the extended emission line region of 18 Seyferts and claim that the range in the observed [N II]/[O II] line ratios can only be reproduced by a range of oxygen abundances going from 0.5 to 3 times solar. By a means of a multi-cloud model, Rodríguez-Ardila et al. (2005) deduce that a nitrogen abundance higher than solar by a factor of at least two would be in agreement with the [N II]+/[O III]+ line ratio observed in the narrow line Seyfert 1 galaxy Mrk 766. Finally, Fields et al. (2005a) use a simple photoionization model of the absorbing gas to find that the strongest absorption system of the narrow line Seyfert 1 (NLS1) galaxy Mrk 1044 has $N/C \gtrsim 4(N/C)_\odot$.

In the circumnuclear gas of the same galaxy, using column density measurements of O VI, C IV, N V, and H I, Fields et al. (2005b) claim that the metallicity is about 5 times solar. This is consistent with expectations from previous studies. Komossa & Mathur (2001), after studying the influence of metallicity on the multi-phase equilibrium in photoionized gas, state that in objects with steep X-ray spectra, such as NLS1s, such an equilibrium is not possible if Z is not supersolar. Studying forbidden emission lines, Nagao et al. (2002) derived $Z \gtrsim 2.5\ Z_\odot$ in NLS1, whereas the gas of broad line Seyferts tends to be slightly less metal rich.

An overabundance of iron was suggested to explain the strong optical Fe II emission in narrow line Seyferts (Collin & Joly 2000) and could provide an explanation for the absorption features around ∼1 keV seen in some of these galaxies (Ulrich et al. 1999; Turner et al. 1999) or for the strength of the FeKα lines (Fabian & Iwasawa 2000). By constraining the relationship between iron abundance and reflection fraction, Lee et al. (1999) show that the observed strong iron line intensity in the Seyfert galaxy MCG−6-30-15 is explained by an iron overabundance by a factor of ∼ 2 in the accretion disk. Ivanov et al. (2003) find values for [Fe/H] derived from the Mg I 1.50 μm line ranging from −0.32 to +0.49, but these values were not corrected for dilution effects from the dusty torus continuum, so are probably underestimated.

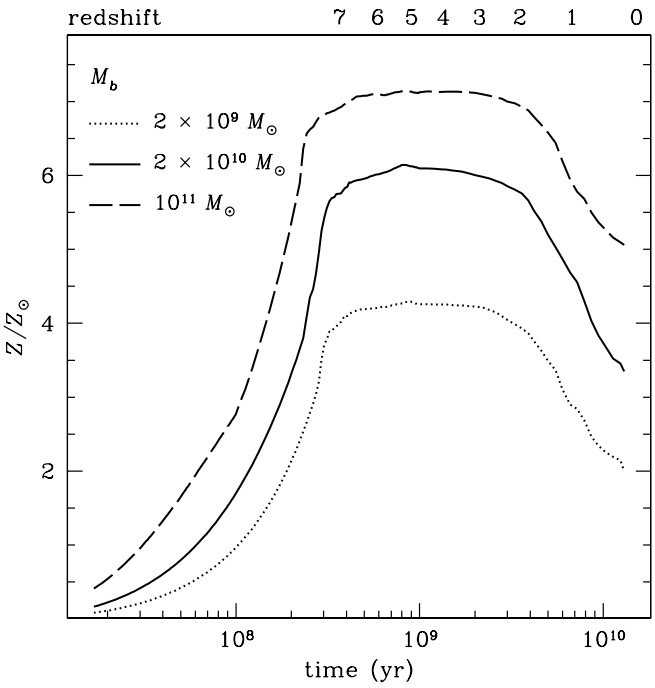

Fig. 7. Evolution with time (bottom axis) and redshift (top axis) of the metallicity in solar units $Z/Z_\odot$. The different curves denote different bulge masses as indicated in the upper left corner.

Table 2. Values assumed by the chemical abundance ratios and by the metallicity in solar units after the wind by bulges of different masses, and the time by which $Z_\odot$ is reached in the different models (last line).

M_b ($M_\odot$)	2×10^9	2×10^{10}	10^{11}
$Z/Z_\odot$	4.23	6.11	7.22
[Fe/H]	+0.83	+0.96	+1.07
[O/H]	+0.18	+0.36	+0.48
[Mg/H]	+0.38	+0.55	+0.69
[Si/H]	+0.79	+0.98	+1.13
[Ca/H]	+0.63	+0.88	+1.06
[O/Fe]	−0.68	−0.60	−0.59
[Mg/Fe]	−0.45	−0.41	−0.38
[Si/Fe]	−0.04	+0.02	+0.06
[Ca/Fe]	−0.19	−0.07	+0.00
[N/H]	+0.28	+0.63	+0.87
[C/H]	+0.15	+0.24	+0.30
[N/C]	+0.13	+0.40	+0.57
$t(Z_\odot)$ (yr)	10^8	6×10^7	3×10^7

Metallicity and elemental abundances

The mean values attained by the metallicity and the examined abundance ratios for $z \lesssim 6$ are resumed in Table 2[3]. Note that all the [α/Fe] ratios are undersolar or solar. Figure 7 shows the evolution with time and redshift of the metallicity Z in solar units, for a standard ΛCDM scenario with $H_0 = 65\ \mathrm{km\,s^{-1}\,Mpc^{-1}}$, $\Omega_M = 0.3$ and $\Omega_\Lambda = 0.7$.

It can be seen that solar metallicities are reached in a very short time, ranging from about 3×10^7 to 10^8 years with decreasing bulge mass (see Table 2). We notice that, due to the α-enhancement typical of spheroids, solar Z is always reached well before solar [Fe/H] is attained, which occurs at times ∼(1−3) × 10^8 years. Then, Z remains approximately constant for the contribution of type Ia SNe and low-and intermediate-mass stars, before declining in the very late phases. The very high metallicities inferred from observations (e.g. Hamann et al. 2002; Dietrich et al. 2003b, their Figs. 5 and 6) are thus very easily achieved. More massive bulges give rise to higher metallicities, which agrees with the statement that more luminous AGNs are more metal rich, if we assume that more massive galaxies are also more luminous. This assumption is supported observationally by e.g. Warner et al. (2003) who find a positive correlation between the mass of the supermassive BH and the metallicity derived from emission lines involving N V in 578 AGNs spanning a wide range in redshifts.

The time dependencies of the abundances of the elements under study for each mass is shown in the Figs. 8 (iron) and 9

[3] We recall that, throughout this paper, we use the standard notation, i.e. for example [Fe/H] = log (Fe/H) − log (Fe/H)$_\odot$.

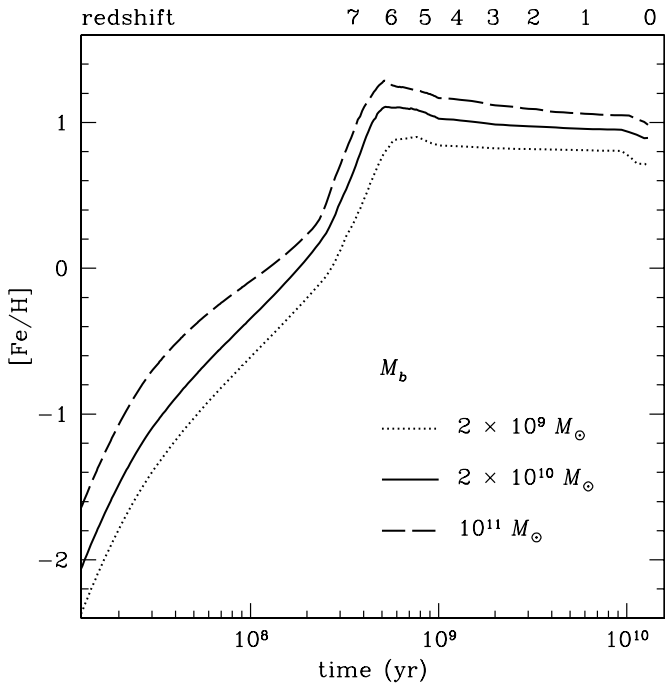

Fig. 8. Evolution with time (bottom axis) and redshift (top axis) of the [Fe/H] abundance ratio in bulges of various masses, as indicated in the lower right corner.

(α-elements, carbon, and nitrogen). A fast increase in the abundances is noticeable at early times, as well as a weak decrease at later times, for all elements and all masses; after the galactic wind, i.e. for $t \gtrsim 0.3$ Gyr (which corresponds to a redshift $z \simeq 6$ in the adopted cosmology) the abundances decrease by a factor smaller than 2. Such a weak decrease occurs over a period of more than 13 Gyr. This can explain the observed constancy of the QSO abundances as a function of redshift (Osmer & Shields 1999).

The elements can be divided according to their behaviour after the wind:

– O and Mg show moderate overabundances relative to solar. They are produced essentially by massive stars ($M > 10\ M_\odot$) on short timescales ($\lesssim 10^7$ years), i.e. almost in lockstep with the star formation. After the galactic wind, therefore, their abundance cannot increase any more because star formation vanishes. They tend instead to be diluted due to the effect of stellar mass loss. In the Galactic bulge at the time of the onset of the wind, Mg is more abundant than O, since although [O/H] is higher at earlier times, it declines very rapidly due to the dependence on metallicity of the adopted O yields (see Ballero et al. 2007a, and references therein). Therefore, we expect the mean value attained by [O/H] after the wind to be lower than that of [Mg/H], which is what we predict. In fact, the mean [O/H] for $z \lesssim 6$ ranges from +0.18 to +0.48 dex, i.e. oxygen is ∼1.5 to 3 times solar, in good agreement with observations (Storchi-Bergmann et al. 1996; Fraquelli & Storchi-Bergmann 2003), and the mean [Mg/H] ranges from +0.38 to +0.69 dex (i.e. 2.5 to 5 times solar), depending on the mass of the host bulge. Finally, we notice that both [O/H] and [Mg/H] reach solar values at times closer to those when $Z = Z_\odot$ for the different models and are therefore better proxies for the metallicity in the bulge with respect to [Fe/H]. This is because the metallicity is dominated by O in the bulge.

– Fe, Si, and Ca are characterised by a bump immediately after the occurrence of the galactic wind, which leads to a significant increase in their abundance, reaching remarkably higher values than in the previous cases ([Fe/H]: +0.83 to +1.07, i.e. ∼7−10 times solar; [Si/H]: +0.79 to +1.13, i.e. ∼6−12 times solar; [Ca/H]: +0.63 to +1.06, i.e. ∼4−10 times solar). This bump is due to the combined effect of the discontinuity caused by the onset of the galactic wind at times of 0.21 to 0.28 Gyr, depending on the model mass, and of the maximum of the type Ia SN rate, occurring at ∼0.2−0.3 Gyr. In fact, these elements are also produced by type Ia SNe (Fe mainly, Si and Ca in part, as they are also produced by type II SNe), which derive from progenitors with masses ranging from 0.8 to 8 $M_\odot$. These elements are restored to the ISM on timescales ranging from ∼30 Myr to a Hubble time. Thus, their abundances could in principle keep increasing even after the star formation has ceased. However, due to the adopted top-heavy IMF ($x_2 = 0.95$), a relatively small fraction of low- and intermediate-mass stars were produced with respect to what we would expect if we had adopted a steeper IMF (see below for a comparison with the IMF of Salpeter 1955), and therefore what we observe is a decrease in the Si, Fe, and Ca abundances after the galactic wind. The estimates for Fe in Seyferts are lower than those calculated here, but we must take several factors into account that would lead to underestimating the Fe produced by stars (e.g. depletion by dust; see Calura et al. 2007b).
– C, as well as O and Mg, is slightly overabundant (∼1.3 to 2.7 times solar). Although it is mostly produced by low- and intermediate-mass stars, in this same range of masses it is also used up to form N. In this case the bump is less pronounced and is mainly caused by the discontinuity induced by the galactic wind, which enhances the relative contribution of low- and intermediate-mass stars.
– Finally, a behaviour similar to Fe is expected from N, since the bulk of this element originates from stars with $M < 8\ M_\odot$. There are, however, two significant differences: first, due its secondary nature, its abundance increases much more rapidly than other elements with time (and with metallicity); and second, this very rapid increase hides the bump at the onset of the wind. We also adopt a primary N production in massive stars (Matteucci 1986; see also Chiappini et al. 2006), but the effects of this choice are only visible before t_{GW}, i.e. when nucleosynthesis from massive stars is active; the decrease of the [N/H] ratio towards earlier times (i.e. lower metallicities) is less rapid. Then, after the wind, the plots with and without primary N essentially overlap. This has already been observed in Ballero et al. (2006) and Ballero et al. (2007a). The mean values attained by [N/H] after the galactic wind ranges from +0.28 to +0.87; i.e., nitrogen is ∼2 to 8 times overabundant with respect to solar. However, [N/H] reaches overabundances of ∼3−10 times solar at its peak. These results agree with the estimates for Seyferts (Schmitt et al. 1994; Storchi-Bergmann et al. 1996; Rodríguez-Ardila et al. 2005).

The difference in behaviour among the α-elements (O, Mg vs. Si, Ca) is even more evident in Fig. 10, where the correlation with mass of the [α/Fe] abundance ratios after the wind is shown. A net separation is present: whereas [Si/Fe] and [Ca/Fe] are approximately solar, O and Mg are underabundant with respect to solar, O showing a more pronounced underabundance. This also agrees with the estimates of a slightly supersolar [Fe/Mg] in QSOs and of its weak correlation with luminosity

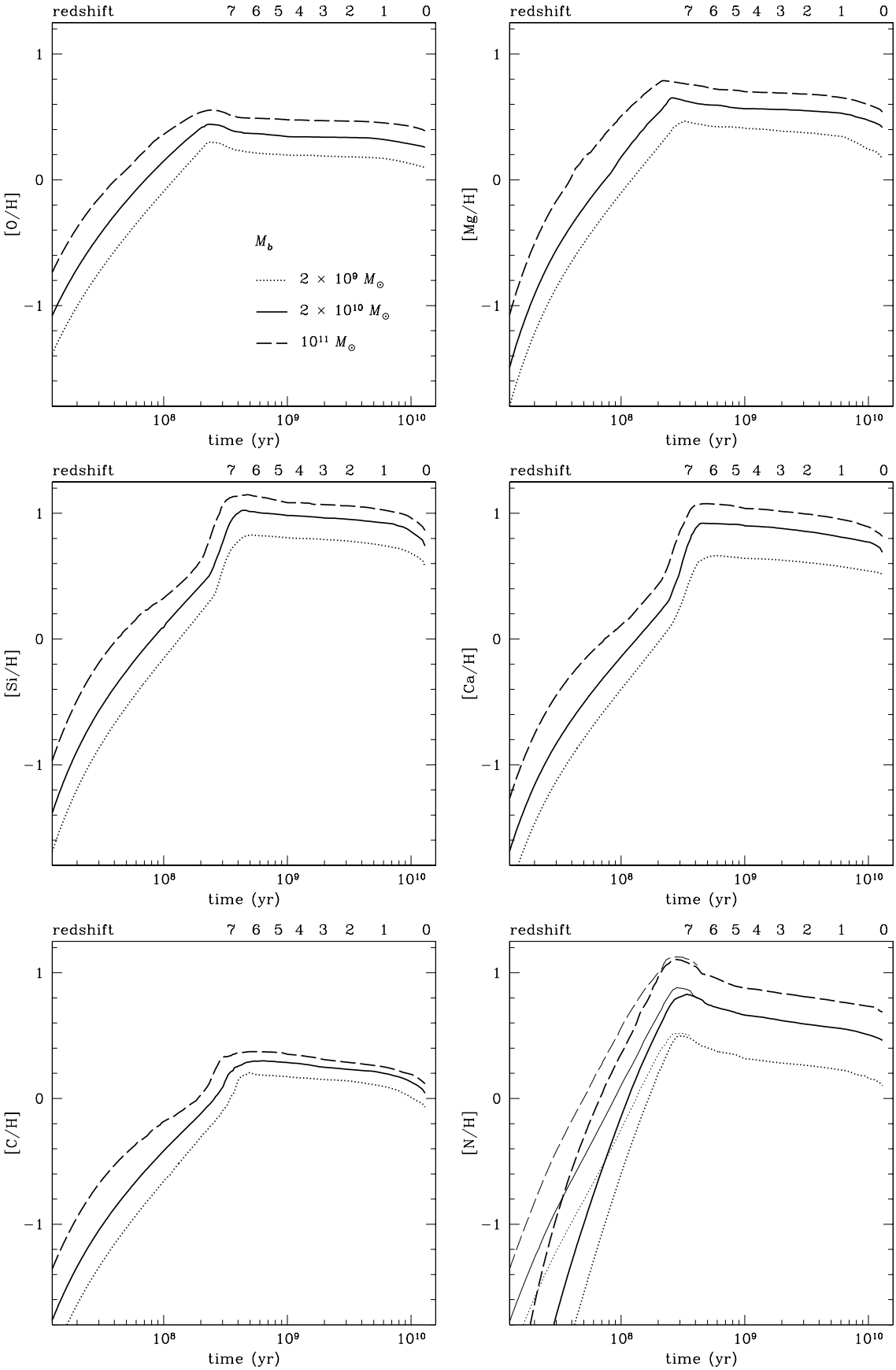

Fig. 9. Evolution with time and redshift of the [X/H] abundance ratios for α-elements (O, Mg, Si, and Ca), C and N in bulges of various masses. The discontinuity at $\sim 2 \times 10^8$ yr in the [Si/H] and [Ca/H] and is due to the occurrence of the galactic wind, which shortly precedes the maximum in the type Ia SN rate. The thin lines in the [N/H] vs. time plot represent the results obtained by adopting primary nitrogen in massive stars, as in Matteucci (1986).

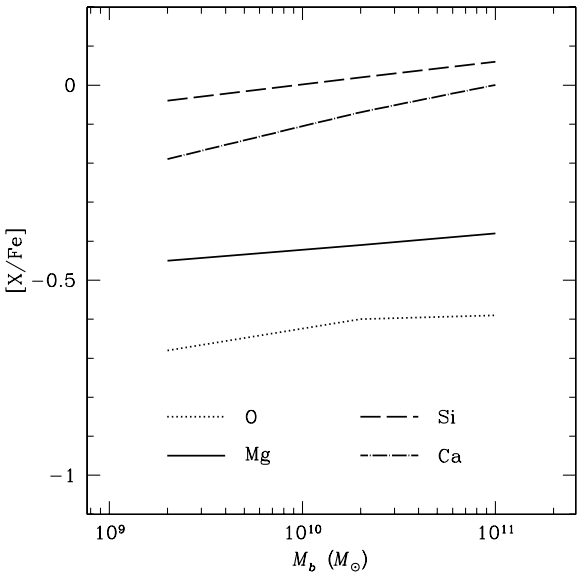

Fig. 10. Correlation with bulge mass of the [X/Fe] abundance ratios for $z \lesssim 6$ for the α-elements O, Mg, Si, Ca.

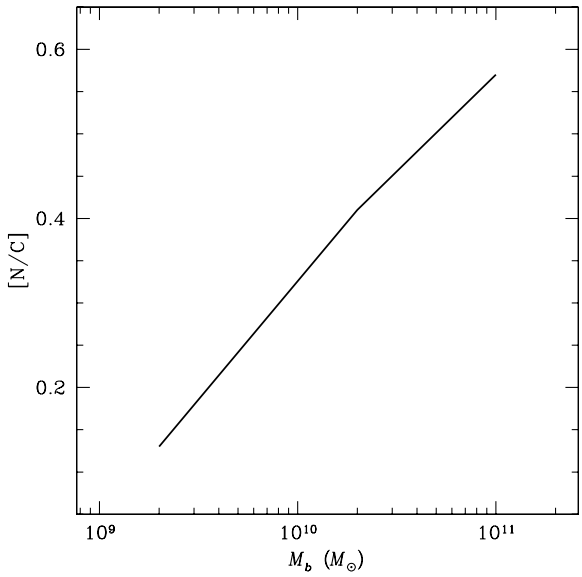

Fig. 11. Correlation with bulge mass of the [N/C] abundance ratio for $z \lesssim 6$.

(Dietrich et al. 2003a) Since both [Fe/H] and [Mg/H] are constant within a factor of 2 up to high redshifts ($z \simeq 6$) and follow the same declining trend with time, we expect this relation to hold for most of the bulge lifetime, which is what is observed for QSOs (Thompson et al. 1999; Iwamuro et al. 2002; Freudling et al. 2003; Dietrich et al. 2003a; Barth et al. 2003; Maiolino et al. 2003; Iwamoto et al. 2004). Here, we predict [Fe/Mg] values ranging from +0.38 to +0.45, the highest values corresponding to less massive galaxies where star formation stops later and type Ia SNe have more time to pollute the bulge ISM.

Figure 11 shows the variation with mass in the [N/C] abundance ratio. The figure illustrates well that this ratio is remarkably sensitive to the galaxy mass, which, as we have seen in Fig. 7, is correlated with the galaxy metallicity. This happens because of the secondary nature of N, which is produced at the expense of C in a fashion proportional to the metallicity of the ISM. The mean [N/C] ratio for $z \lesssim 6$ ranges from +0.13 to +0.57 depending on the bulge mass; i.e., the N/C ratio is ∼1.4 to 3.7 times solar. If we consider the amount of variation in the two abundances, these values are consistent with the estimates of Fields et al. (2005a).

Finally, we briefly compare the results obtained with the top-heavy IMF ($x_2 = 0.95$) with those we obtain if instead we adopt $x_2 = 1.35$ (Salpeter 1955). In Ballero et al. (2007a) this IMF was excluded on the basis of the stellar metallicity distribution, since with our model the Salpeter index for massive stars gives rise to a distribution that is too metal-poor with respect to the observed ones (Zoccali et al. 2003; Fulbright et al. 2006), and Ballero et al. (2007b) seem to further confirm this point. However, Pipino et al. (2007) show that a hydrodynamical model for ellipticals can be adapted to the galactic bulge and, with a spherical mass distribution, it reproduces the above-mentioned metallicity distributions with a Salpeter IMF. Furthermore, as we shall show (see Sect. 4.5), the $(B - I)$ colours and bulge K-band luminosity are better reproduced by a Salpeter IMF above 1 $M_\odot$. Therefore a brief comparison is useful.

In Fig. 12 we show the evolution with time and redshift of the abundance ratios relative to hydrogen for some of the elements considered, namely Fe, O, and N. We find similar trends for all the elements. However, in the Salpeter case, the abundances at the wind are lower than with a top-heavy IMF, because the enrichment from massive stars is lower. Then, those elements that are produced mainly by low- and intermediate-mass stars (in this case, Fe and N) keep increasing after the wind until they reach a maximum value, which is generally slightly higher than what is obtained with the top-heavy IMF, and their abundance stops increasing. The bump in the [Fe/H] is ∼0.1 dex larger because the production of type Ia SN progenitors is favoured in this case. In contrast, oxygen abundance decreases steadily after the wind because it is essentially produced by massive stars and its value remains below the one calculated with the top-heavy IMF. The abundance ratios are still almost constant for $z \lesssim 6$, and their mean values are, respectively:

- [Fe/H] = 0.79 to 1.08, i.e. 6 to 12 times solar;
- [O/H] = −0.09 to 0.27, i.e. 0.8 to 2 times solar;
- [N/H] = 0.29 to 0.84, i.e. 2 to 7 times solar.

The values for Fe are thus again overestimated with respect to observations, but as said, the latter are not corrected for Fe depletion by dust or dilution by dusty torus continuum (Ivanov et al. 2003). The total metallicity Z ranges from about 3.5 to 6.5 solar, i.e. slightly less than in the top-heavy IMF case, but still in agreement with observational estimates, as well as the N and O abundances.

We point out that the adoption of a Salpeter IMF would only result into a small change in the quantities calculated previously, i.e. mass accretion rate, luminosity, energetics, and final black hole mass. The accretion rates of Eddington and Bondi do not depend on the adopted IMF. A steeper IMF only slightly shifts the time of occurrence of the wind of a few tens Myrs ahead, thus prolonging the Eddington-limited accretion phase that, as we said, is the phase when most of accretion and shining occurs. This will lead to a higher BH mass; however, the final BH masses increase by only about 10%.

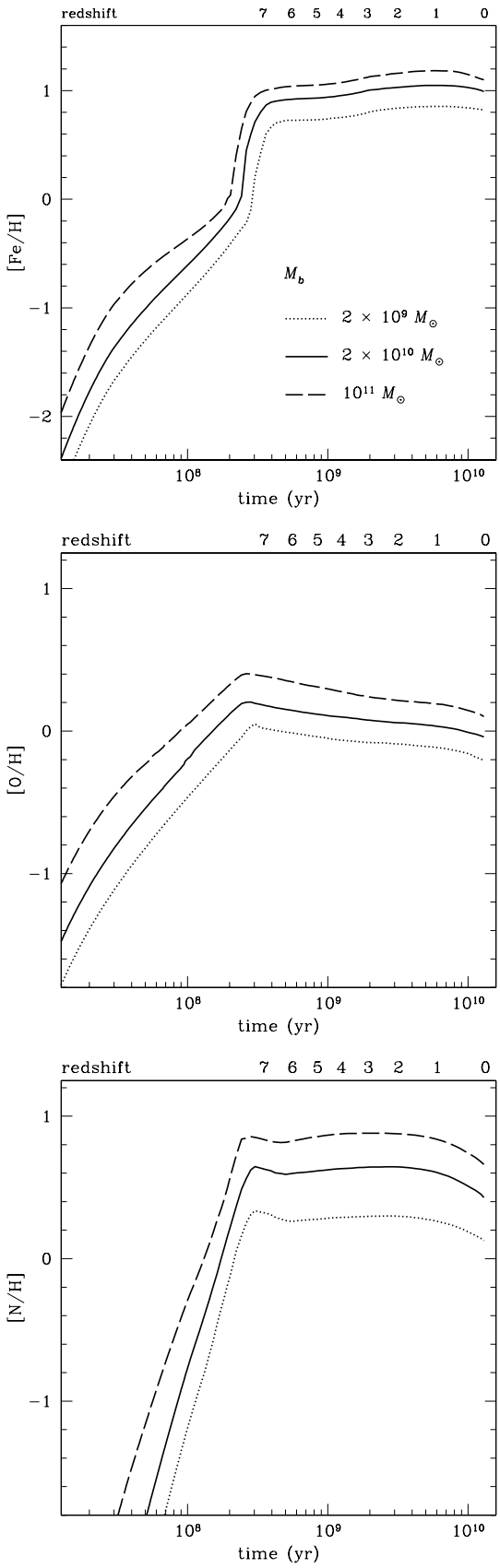

Fig. 12. Evolution with time and redshift of the [X/H] abundance ratios for Fe, Mg, and N in bulges of various masses and the adoption of a Salpeter (1955) IMF above 1 $M_\odot$. The discontinuity at $\sim 3 \times 10^8$ yr in the [Fe/H] and [Si/H] is due to the occurrence of the galactic wind, which shortly precedes the maximum in the type Ia SN rate.

4.5. Bulge colours and the colour-magnitude relation

In this section, we present our results for the spectro-photometric evolution of the three bulge models studied in this paper. The photometrical evolution of Seyfert galaxies, which requires modeling of the AGN continuum and, for type 2 Seyferts, of the dusty torus, is not treated at present and may be the subject of a forthcoming paper.

In Fig. 13, we show the predicted time evolution of the $(U - B)$ and $(B - K)$ colours for the three bulge models studied in this work. We assume an IMF with $x_1 = 0.33$ for stars with masses M in the range $0.1 \leq M/M_\odot \leq 1$ and $x_2 = 0.95$ for $M > 1\ M_\odot$. At all times, higher bulge masses correspond to redder colours, owing both to a higher metallicity and to an older age. This is consistent with the popular "downsizing" picture of galaxy evolution, according to which the most massive galaxies have evolved faster than the less massive ones (Matteucci 1994; Calura et al. 2007c).

In Fig. 14, we show how the assumption of two different IMFs affects the predicted evolution of the $(U - B)$ and $(B - K)$ colours, for a bulge of mass $M_\mathrm{b} = 2 \times 10^{10}\ M_\odot$. We compare the colours calculated with the IMF presented in Sect. 2.1 with the ones calculated by assuming an IMF with $x_1 = 0.33$ for stars with masses M in the range $0.1 \leq M/M_\odot \leq 1$ and $x_2 = 1.35$ for $M > 1\ M_\odot$. It is interesting to note how, at most of the times, the assumption of a flatter IMF for stars with masses $M > 1\ M_\odot$ implies redder colours. This is due primarily to a metallicity effect, since a flatter IMF implies a larger number of massive stars and a larger fraction of O (the element dominating the metal content) restored into the ISM at all times.

In Fig. 15, we show the colour-magnitude relation (CMR) predicted for our bulge models and compared to the data from Itoh & Ichikawa (1998, panel a), and Peletier & Balcells (1996, panels b and c). Itoh & Ichikawa measured the colours of 9 bulges in a fan-shaped aperture opened along the minor axis, in order to minimize the effects of dust extinction. In panel a of Fig. 15 we show the linear regression to the data observed by Itoh & Ichikawa (1998) and the dispersion.

Peletier & Balcells (1996) determined the colours for a sample of local bulges, for which they estimated that the effect of dust reddening is negligible. Of the sample studied by Peletier & Balcells (1996), we consider a subsample of 17 bulges here, for which Balcells & Peletier (1994) have published the absolute R magnitudes. This allows us to plot an observational CMR.

The predicted CMR has been calculated by adopting two different IMFs, i.e. with $x_2 = 0.95$ and $x_2 = 1.35$, represented in Fig. 15. From the analysis of the I vs. $(B - I)$ plot, we note that the adoption of a flatter IMF leads to an overestimation of the predicted $(B - I)$ colours; in fact, the predictions for the flatter IMF lie above the upper dotted lines, representing the upper limits for the data observed by Itoh & Ichikawa (1998). On the other hand, the predictions computed with an IMF with $x_2 = 1.35$ are consistent with the available observations.

From the analysis of the R vs. $(U - R)$ diagram, we note that our predictions computed assuming $x_2 = 1.35$ are consistend with the observations, in particular for the bulge models of masses $2 \times 10^{10}\ M_\odot$ and $10^{11}\ M_\odot$. For the lowest mass bulge, corresponding to the highest absolute R magnitude, the $(U - R)$ colour seems to be overestimated. In Table 3, we present our results for the predicted present-day colours for the bulge model of mass $2 \times 10^{10}\ M_\odot$, computed for two different IMFs, compared to observational values for local bulges derived by various authors. The present-day values are computed at 13.7 Gyr. Note that, for each colour, the observational values represent the

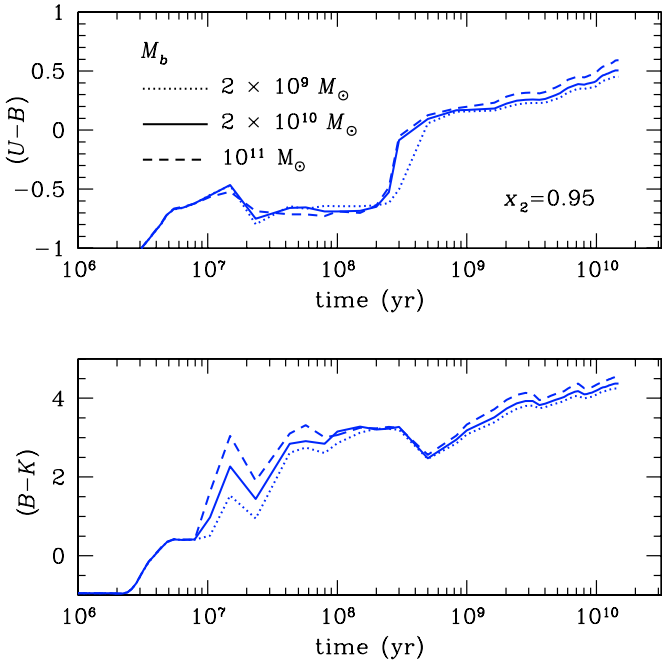

Fig. 13. Evolution of the predicted $(U-B)$ (*upper panel*) and $(B-K)$ (*lower panel*) colours for bulge models of three different masses (*dotted line:* $M_b = 2\times10^9\ M_\odot$; *solid line:* $M_b = 2\times10^{10}\ M_\odot$; *dashed line:* $M_b = 10^{11}\ M_\odot$), assuming an IMF with $x_2 = 0.95$.

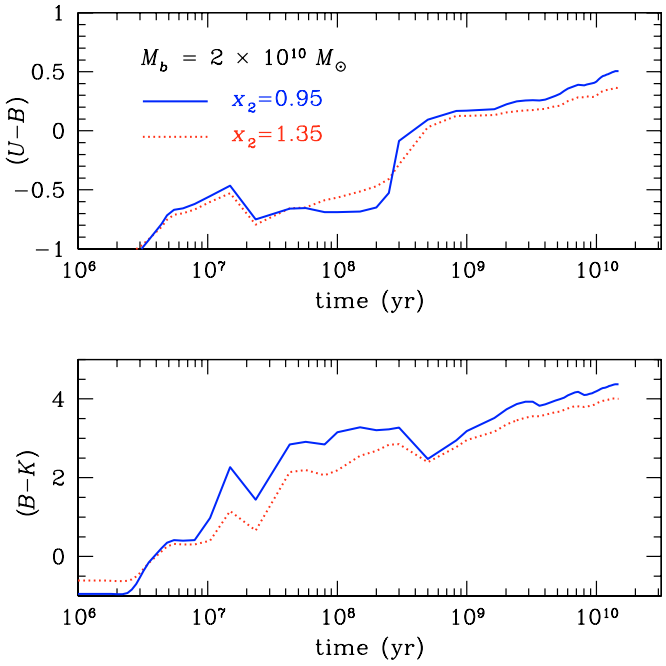

Fig. 14. Evolution of the predicted $(U-B)$ (*upper panel*) and $(B-K)$ (*lower panel*) colours for a bulge model of mass $M_b = 2\times10^{10}\ M_\odot$ assuming two different IMFs. The solid lines represent the colours computed by assuming $x_2 = 0.95$, whereas the dotted lines are computed assuming $x_2 = 1.35$.

lowest and highest observed values reported by the authors. The values we predict are compatible with the observations of local bulges, which show a considerable spread. However, the sample of bulges considered here seems to be skewed towards high-mass

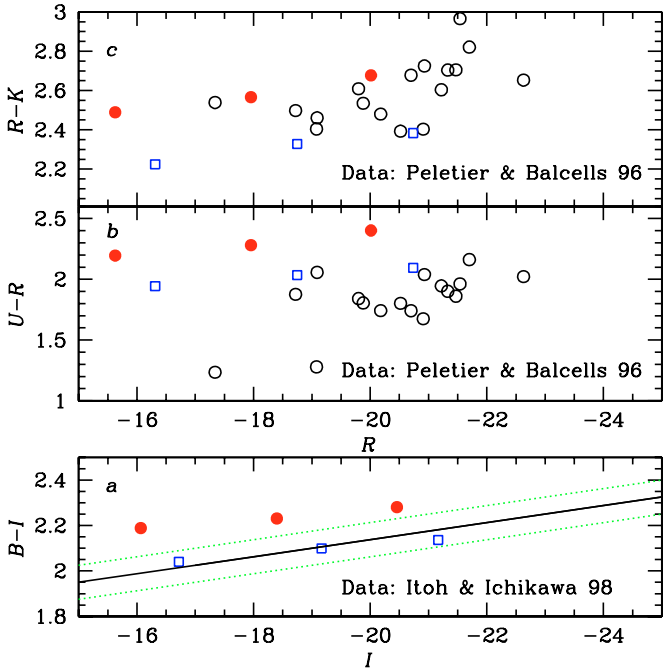

Fig. 15. Predicted and observed colour-magnitude relation for bulges. The solid line and the dotted lines are the regression and the dispersion of CMR observed by Itoh & Ichikawa (1998), respectively. The solid circles and open squares are our predictions for the three bulge models studied in this paper, computed by assuming for the IMF $x_2 = 0.95$ and $x_2 = 1.35$, respectively. Panel **b)** R vs. $(U-R)$ diagram. The open circles are the data by Peletier & Balcells (1996). Solid circles and open squares as in panel **a)**. Panel **c)** R vs. $(R-K)$ diagram. Open circles, solid circles, and open squares as in panel **a)**.

bulges, making it difficult to infer the trend of the R vs. $(U-R)$ for magnitudes $R < -16$ mag. On the other hand, the predictions computed by assuming $x_2 = 0.95$ seem to produce $(U-R)$ colours that are much too high with respect to the observations. Finally, the R vs. $(R-K)$ diagram does not allow us to draw any firm conclusion on the slope of the IMF.

From the combined study of the I vs. $(B-I)$, R vs. $(U-R)$ and R vs. $(R-K)$ diagrams, we conclude that the observational data for local bulges seem to disfavour IMF flatter than $x_2 = 1.35$ in the stellar mass range $1 \le M/M_\odot \le 80$. In Table 3, we present our results for the predicted present day colours for the three bulge models presented in this paper, computed for two different IMFs. The present-day values are computed at 13.7 Gyr. In the same table, we show the observational data of Peletier & Balcells (1996) and of Galaz et al. (2006), who estimate that dust effects should be small for their sample, with an upper limit on the extinction of 0.3 mag. Note that, for each colour, the observational values represent the lowest and highest observed values reported by the authors.

For the model with mass comparable to the one of the bulge of the Milky Way galaxy, i.e. the one with a total mass $M = 2\times10^{10}\ M_\odot$, with the assumption of an IMF with $x_2 = 0.95$, we predict a present K-band luminosity $L_{\mathrm{Bul},K} = 4.5\times10^9\ L_\odot$. Existing observational estimates of the K-band luminosity of the bulge indicate values $0.96\times10^{10} \le L_{\mathrm{Bul},K,\mathrm{obs}} \le 1.8\times10^{10}\ L_\odot$ (Dwek et al. 1995; Launhardt et al. 2002), i.e. at least a factor of 2 higher than the estimate obtained with our model. By adopting an IMF with $x_2 = 1.35$, we obtain $L^{x=1.35}_{\mathrm{Bul},K} = 7.6\times10^9\ L_\odot$, in better agreement with the observed range of values.

Table 3. Predicted colours for the Galactic bulge assuming two different IMFs, compared to observational values of local bulges from various sources (*a*: Balcells & Peletier 1994; *b*: Galaz et al. 2006).

Photometric properties of the Galactic Bulge

		$(B-R)$	$(U-R)$	$(R-K)$
Observed	(*a*)	1.27–1.6	1.24–2.16	2.39–2.97
	(*b*)	0.5–2.18		
Predicted	($x = 1.35$)	1.64–1.71	1.94–2.09	2.22–2.38
	($x = 0.95$)	1.75–1.83	2.20–2.40	2.49–2.68

5. Summary and conclusions

We made use of a self-consistent model of galactic evolution which reproduces the main observational features of the Galactic bulge (Ballero et al. 2007a) to study the fueling and the luminous output of the central supermassive BH in spiral bulges, as fed by the stellar mass loss and cosmological infall, at a rate given by the minimum between the Eddington and Bondi accretion rates. A realistic galaxy model was adopted to estimate the gas binding energy in the bulge, and the combined effect of AGN and supernova feedback was taken into account as contributing to the thermal energy of the interstellar medium. We also investigated the chemical composition of the gas restored by stars to the interstellar medium. Assuming that the gas emitting the broad and narrow lines observed in Seyfert spectra is well mixed with the bulge interstellar medium, we have made specific predictions regarding Seyfert metallicities and abundances of several chemical species (Fe, O, Mg, Si, Ca, C and N), and their redshift evolution. Finally, we calculated the evolution of the $(B-K)$ and $(U-B)$ colours, the present-day bulge colours and K-band luminosity and the color-magnitude relation, and discussed their dependence on the adopted IMF.

Our main results can be summarised as follows:

1. The AGN goes through a first phase of Eddington-limited accretion and a second phase of Bondi-limited accretion. Most of the fueling (and of the shining) of the AGN occurs at the transition between the two phases, which approximately coincides with the occurrence of the wind. Within a factor of two, the final black hole mass is reached in a fraction of the bulge lifetime ranging from 2 to 5%.
2. The peak bolometric luminosities predicted for AGNs residing in the bulge of spiral galaxies are in good agreement with those observed in Seyfert galaxies ($\simeq 10^{42}$–10^{44} erg s^{-1}). At late times, the model nuclear luminosities (produced by accretion of the mass return from the passively aging stellar populations) are $<10^{42}$ erg s^{-1}, and would be further reduced by a factor $\sim$0.01 when considering ADAF (or its variants) accretion regimes. To recover an agreement with the luminosities of local Seyferts, it is necessary to assume a rejuvenation event in the past 1–2 Gyr.
3. The feedback from the central AGN is not in any case the main one responsible for triggering the galactic wind, since its contribution to the thermal energy is at most comparable to that of the supernova feedback.
4. The proportionality between the mass of the host bulge and that of the central black hole is reproduced very well without the need to switch off the accretion ad hoc. We derived an approximate relation of $M_{\rm BH} \approx 0.0009 M_{\rm b}$, consistent with recent estimates (McLure & Dunlop 2002; Marconi & Hunt 2003; Häring & Rix 2004).
5. The massive amounts of star formation (several thousands solar masses a year) needed to produce the observed line strengths, dust content, and metallicities of Seyfert galaxies are easily attained. Due to such a high star formation rate, solar metallicity is reached in less than 10^8 yr, and solar abundances for the elements we considered are reached in a few hundred million years. This naturally explains the high metallicities and abundances inferred for Seyfert galaxies in analogy with QSOs.
6. After the first $\sim$300 million years, the interstellar medium in the bulge reaches overabundances of up to one order of magnitude for N, Fe, Si, Ca, up to 5 times solar for Mg, and 3 times solar for C and O. This is roughly consistent with the estimates for Fe, N, and O in the broad and intrinsic narrow line regions of Seyfert galaxies. The slightly supersolar [Fe/Mg] and its weak dependence on the galaxy luminosity (mass) are recovered. These results remain essentially unchanged if we adopt a Salpeter (1955) stellar initial mass function.
7. The mean value assumed by the [N/C] abundance ratio is very sensitive to the galaxy mass, due to the sensitivity of N to metallicity. The calculated values are consistent with recent estimates (Fields et al. 2005a).
8. Higher bulge masses imply redder colours, in agreement with the downsizing picture of galaxy evolution. A flatter IMF gives rise to a redder bulge. While the present-day bulge colours are well fitted both by a top-heavy ($x_2 = 0.95$) and a Salpeter ($x_2 = 1.35$) IMF, the latter is required in order to achieve better agreement with the colour-magnitude relation and the present-day K-band luminosity of the bulge.

Acknowledgements. S.K.B. wishes to acknowledge Antonio Pipino for interesting suggestions and discussions. The authors thank the referee Mathias Dietrich for indicating useful references.

Appendix A: The disk gravitational energy contributions

In this paper, we assumed spherical symmetry for the gas distribution in the bulge in order to estimate its binding energy of the gas itself. Thus, the contribute of the spherical stellar bulge and the spherical dark matter halo are given by the elementary expressions (17) and (18).

A more complicate case is represented by the disk-gas interaction. In fact, one could suppose that a 2-dimensional integral, involving special functions must be evaluated, because of the disk geometry. However, this is not the case: in fact, if each gas element is displaced radially from r to $r_{\rm t}$, then

$$\begin{aligned}\Delta E_{\rm gd} &= \int_0^{r_{\rm t}} \rho_{\rm g}(r) r^2 {\rm d}r \int_{4\pi} {\rm d}\Omega [\phi_{\rm d}(\boldsymbol{e}_r r_{\rm t}) - \phi_{\rm d}(\boldsymbol{e}_r r)] \\ &= 4\pi \int_0^{r_{\rm t}} \rho_{\rm g}(r) r^2 [\bar{\phi}_{\rm d}(r_{\rm t}) - \bar{\phi}_{\rm d}(r)] {\rm d}r \end{aligned} \quad (A.1)$$

where

$$\bar{\phi}_{\rm d}(r) = \frac{1}{4\pi} \int_{4\pi} \phi_{\rm d}(\boldsymbol{e}_r r) {\rm d}\Omega \quad (A.2)$$

is the angular averaged potential, and $\boldsymbol{e}_r$ the radial unit vector. It is trivial to prove by direct evaluation that the angular mean of the potential of a generic density distribution is also the (spherical) potential of the angular averaged density. Of course, this result can also be obtained in a more elegant way by considering the angular mean of the expansion of the potential in spherical harmonics (e.g., Binney & Tremaine 1987), so that all the terms vanish, except the monopole. An identical argument also holds

in the case of the computation of the virial trace. In fact, from $\boldsymbol{x} = \boldsymbol{e}_r r$ it follows that

$$W_{\rm bd} = -\int \rho_{\rm g}\langle \boldsymbol{x}, \nabla\phi_{\rm d}\rangle {\rm d}^3\boldsymbol{x} = -4\pi \int \rho_{\rm g}(r)\frac{{\rm d}\bar{\phi}_{\rm d}(r)}{{\rm d}r} r^3 {\rm d}r. \quad (A.3)$$

The surface density of a razor-thin axisymmetric disk in spherical coordinates is

$$\Sigma(r,\vartheta,\varphi) = \frac{\Sigma_{\rm d}(r\sin\vartheta)\delta(\cos\vartheta)}{r}, \quad (A.4)$$

so that

$$\bar{\rho}_{\rm d}(r) = \frac{1}{4\pi}\int_{4\pi}\Sigma(r,\vartheta,\varphi){\rm d}\Omega = \frac{\Sigma_{\rm d}(r)}{2r}\cdot \quad (A.5)$$

For the exponential disk in Eq. (14), we then obtain

$$\bar{\phi}_{\rm d}(r) = -\frac{GM_{\rm d}}{r}\left(1 - {\rm e}^{-r/R_{\rm d}}\right), \quad (A.6)$$

so that integrations in (A.1) and (A.3) reduce to

$$\widetilde{\Delta E_{\rm gd}} = \frac{\delta + (1-h)(1-{\rm e}^{-\delta/h})}{1+\delta} + \frac{{\rm e}^{1/h}}{h}\left[E_i\left(-\frac{1}{h}\right) - E_i\left(-\frac{1}{h} - \frac{1}{\delta}\right)\right] \quad (A.7)$$

and

$$\widetilde{W_{\rm bd}} = -\frac{1}{h} - \frac{{\rm e}^{1/h}(1+h)}{h^2}E_i\left(-\frac{1}{h}\right) \quad (A.8)$$

where $h \equiv R_{\rm d}/r_{\rm b}$, $\delta \equiv r_{\rm t}/r_{\rm b}$, and $E_i(-x) = -\int_r^\infty {\rm e}^{-t}t^{-1}{\rm d}t$ is the exponential integral.

References

Adams, T. F. 1977, ApJS, 33, 19
Angeletti, L., & Giannone, P. 1990, A&A, 234, 53
Arimoto, N., & Yoshii, Y. 1987, A&A, 173, 23
Balcells, M., & Peletier, R. F. 1994, AJ, 107, 135
Baldwin, J. A., Ferland, G. J., Korista, K. T., Hamann, F., & LaCluyzé, A. 2004, ApJ, 615, 610
Ballero, S. K., Matteucci, F., & Chiappini, C. 2006, NewA, 11, 306
Ballero, S. K., Matteucci, F., Origlia, L., & Rich, R. M. 2007a, A&A, 467, 123
Ballero, S. K., Kroupa, P., & Matteucci, F. 2007b, A&A, 467, 117
Barth, A. J., Martini, P., Nelson, C. H., & Ho, L. C. 2003, ApJ, 594, L95
Bentz, M. C., Hall, P. B., & Osmer, P. S. 2004, AJ, 128, 561
Bertin, G., Saglia, R. P., & Stiavelli, M. 1992, ApJ, 384, 423
Binney, J., & Tremaine, S. 1987, Galactic Dynamcis (Princeton NJ: Princeton University Press)
Blain, A. W., Smail, I., Ivison, R. J., Kneib, J.-P., & Frayer, D. T. 2002, Phys. Rep., 369, 111
Bondi, H. 1952, MNRAS 112, 195
Brandt, W. N., & Hasinger, G. 2005, ARA&A, 43, 827
Calura, F., & Matteucci, F. 2003, ApJ, 596, 734
Calura, F., & Matteucci, F. 2006, ApJ, 652, 889
Calura, F., Matteucci, F., & Menci, N. 2004, MNRAS, 353, 500
Calura, F., Matteucci, F., & Tozzi, P. 2007a, MNRAS, 378, L11
Calura, F., Pipino, A., & Matteucci, F. 2007b, A&A, accepted [arXiv:0706.2197v1]
Calura, F., Jimenez, R., Panter, B., Matteucci, F., & Heavens, A. F. 2007c, MNRAS, submitted [arXiv:0707.1345v2]
Cavaliere, A., & Vittorini, V. 1998, in The Young Universe: Galaxy Formation and Evolution at Intermediate and High Redshift, ed. S. D'Odorico, A. Fontana, & E. Giallongo, ASP Conf. Ser., 146, 26
Chiappini, C., Matteucci, F., & Gratton, R. 1997, ApJ, 477, 765
Chiappini, C., Romano, D., & Matteucci, F. 2003, MNRAS, 339, 63
Cimatti, A., Pozzetti, L., Mignoli, M., et al. 2002, A&A, 391, L1
Cioffi, D. F., McKee, C. F., & Bertschinger, E. 1988, ApJ, 334, 252
Ciotti, L., & Ostriker, J. P. 1997, ApJ, 487, L105
Ciotti, L., & Ostriker, J. P. 2001, ApJ, 551, 131
Ciotti, L., & Ostriker, J. P. 2007, ApJ, 665, 1038
Collin, S., & Joly, M. 2000, NewAR, 44, 531
Cox, D. P. 1972, ApJ, 178, 159
Cox, P., Omont, A., Djorgovski, S. G., et al. 2002, A&A, 387, 406
Dietrich, M., Hamann, F., Appenzeller, I., & Vestergaard, M. 2003a, ApJ, 596, 817
Dietrich, M., Hamann, F., Shields, J. C., et al. 2003b, ApJ, 589, 722
Di Matteo, T., Croft, R. A. C., Springel, V., & Hernquist, L. ApJ, 593, 56
Di Matteo, T., Springel, V., & Hernquist, L. 2005, Nature, 433, 604
D'Odorico, V., Cristiani, S., Romano, D., Granato, G. L., & Danese, L. 2004, MNRAS 351, 976
Dunlop, J. S., McLure, R. J., Kukula, M. J., et al. 2003, MNRAS, 340, 1095
Dwek, E., Arendt, R. G., Hauser, M. G., et al. 1995, ApJ, 445, 716
Fabian, A. C., & Iwasawa, K. 2000, AdSpR, 25, 471
Ferrarese, L., & Merritt, D. 2000, ApJ, 539, L9
Ferrarese, L., Pogge, R. W., Peterson, B. M., et al. 2001, ApJ, 555, L79
Fields, D. L., Mathur, S., Pogge, R. W., Nicastro, F., & Komossa, S. 2005a, ApJ, 620, 183
Fields, D. L., Mathur, S., Pogge, R. W., et al. 2005b, ApJ, 634, 928
Ford, H. C., Tsvetanov, Z. I., Ferrarese, L., & Jaffe, W. 1998, in The Central Regions of the Galaxy and galaxies, ed. Y. Sofue, IAU Symp., 184, 377
François, P., Matteucci, F., Cayrel, R., et al. 2004, A&A, 421, 613
Fraquelli, H. A., & Storchi-Bergmann, T. 2003, BASBr, 23, 150
Freudling, W., Corbin, M. R., & Korista, K. T. 2003, ApJ, 587, L67
Friaça, A. C. S., & Terlevich, R. J. 1998, MNRAS, 298, 399
Fulbright, J. P., McWilliam, A., & Rich, R. M. 2006, ApJ, 636, 821
Fulbright, J. P., McWilliam, A., & Rich, R. M. 2007, ApJ, 661, 1152
Galaz, G., Villalobos, A., Infante, L., & Donzelli, C. 2006, AJ, 131, 2035
Gebhardt, K., Bender, R., Bower, G., et al. 2000a, ApJ, 539, L13
Gebhardt, K., Kormendy, J., Ho, L. C., et al. 2000b, ApJ, 543, L5
Genzel, R., Baker, A. J., Tacconi, L. J., et al. 2003, ApJ, 584, 633
González Delgado, R. M., Heckman, T., Leitherer, C., et al. 1998, ApJ, 505, 174
Granato, G. L., De Zotti, G., Silva, L., Bressan, A., & Danese, L. 2004, ApJ, 600, 580
Groenewegen, M. A. T., & Blommaert, J. A. D. L. 2005, A&A, 443, 143
Gu, Q., Melnick, J., Cid Fernandes, R., et al. 2006, MNRAS, 366, 480
Haiman, Z., Ciotti, L., & Ostriker, J. P. 2004, ApJ, 606, 763
Hamann, F., & Ferland, G. 1993, ApJ, 418, 11
Hamann, F., & Ferland, G. 1999, ARA&A, 37, 487
Hamann, F., Korista, K. T., Ferland, G. J., Warner, C., & Baldwin, J. 2002, ApJ, 564, 592
Hamann, F., Dietrich, M., Sabra, B., et al. 2003, in CNO in the Universe, ed. C. Charbonnel, D. Schaerer, & G. Meynet, ASP Conf. Ser., 304, 236
Hamann, F., Dietrich, M., Sabra, B., & Warner, C. 2004, in Origin and Evolution of the Elements, ed. A. McWilliam, & M. Rauch, Carnegie Observatories Astrophysics Ser., 4, 443
Häring, N., & Rix, H.-W. 2004, ApJ, 604, L89
Hernquist, L. 1990, ApJ, 356, 359
Ho, L. C. 1999, ApJ, 516, 672
Ho, L. C., Filippenko, A. V., & Sargent, W. L. W. 1997, ApJ, 487, 568
Itoh, N., & Ichikawa, T. 1998, IAUS, 184, 55
Ivanov, V. D., Alonso-Herrero, A., & Rieke, M. J. 2003, in Star Formation through Time, ed. E. Pérez, R. M. González Delgado, & G. Tenorio-Tagle, ASP Conf. Ser., 297, 165
Iwamuro, F., Motohara, K., Maihara, T., et al. 2002, ApJ, 565, 63
Iwamuro, F., Kimura, M., Eto, S., et al. 2004, ApJ, 614, 69
Jiang, L., Fan, X., Vestergaard, M., et al. 2007, AJ, 134, 1150
Jimenez, R., Padoan, P., Matteucci, F., & Heavens, A. F. 1998, MNRAS, 299, 123
Jimenez, R., MacDonald, J., Dunlop, J. S., Padoan, P., & Peacock, J. A. 2004, MNRAS, 349, 240
Kaspi, S., Smith, P. S., Netzer, H., et al. 2000, ApJ, 533, 631
Kodama, T. 1997, Ph.D. Thesis, University of Tokio
Komossa, S., & Mathur, S. 2001, A&A, 374, 914
Korista, K., Kodituwakku, N., Corbin, M., & Freudling, W. 2004, in AGN Physics with the SDSS, ed. G. T. Richards, & P. B. Hall, ASP Conf. Ser., 311, 415
Kormendy, J., & Richstone, D. 1995, ARA&A, 33, 581
Kurk, J. D., Walter, F., Fan, X., et al. 2007, ApJ, in press [arXiv:0707.1662]
Kurucz, R. L. 1992, IAUS, 149, 225
Laor, A. 2001, ApJ, 553, 677
Launhardt, R., Zylka, R., & Mezger, P. G. 2002, A&A, 384, 112
Lecureur, A., Hill, V., Zoccali, M., et al. 2007, A&A, 465, 799
Lee, J. C., Fabian, A. C., Brandt, W. N., Reynolds, C. S., & Iwasawa, K. 1999, MNRAS, 310, 973
MacArthur, L. A., Ellis, R. S., Treu, T. U. V., Bundy, K., & Moran, S. 2007, ApJ, submitted [arXiv:0711.0238]
MacKenty, J. W. 1990, ApJS, 72, 231

Magorrian, J., Tremaine, S., Richstone, D., et al. 1998, AJ, 115, 2285
Maiolino, R., Cox, P., Caselli, P., et al. 2005, A&A, 440, L51
Maiolino, R., Juarez, Y., Mujica, R., Nagar, N. M., & Oliva, E. 2003, ApJ, 596, L155
Marconi, A., & Hunt, L. 2003, ApJ, 589, 21
Markowitz, A., Edelson, R., Vaughan, S., et al. 2003, ApJ, 593, 96
Mathur, S. 2000, NewAR, 22, 469
Matteucci, F. 1986, MNRAS, 221, 911
Matteucci, F. 1992, ApJ, 397, 32
Matteucci, F. 1994, A&A, 288, 57
Matteucci, F., & Padovani, P. 1993, ApJ, 419, 485
Matteucci, F., & Recchi, S. 2001, ApJ, 558, 351
Matteucci, F., & Tornambè, A. 1987, A&A, 185, 51
McLure, R. J., & Dunlop, J. S. 2002, MNRAS, 331, 795
Monaco, P., Salucci, P., & Danese, L. 2000, MNRAS, 311, 279
Nagao, T., Marconi, A., & Maiolino, R. 2006, A&A, 447, 157
Nagao, T., Murayama, T., Shioya, Y., & Taniguchi, Y. 2002, ApJ, 575, 721
Narayan, R., & Yi, I. 1994, ApJ, 428, L13
Nelson, C. H., Green, R. F., Bower, G., Gebhardt, K., & Weistrop, D. 2004, ApJ, 615, 652
Nomoto, K., Thielemann, F. K., & Yokoi, K. 1984, ApJ, 286, 644
Onken, C. A., Ferrarese, L., Merritt, D., et al. 2004, ApJ, 615, 645
Origlia, L., & Rich, R. M. 2004, AJ, 127, 3422
Origlia, L., Rich, R. M., & Castro, S. 2002, AJ, 123, 1559
Origlia, L., Valenti, E., & Rich, R. M. 2005, MNRAS, 256, 127
Osmer, P. S., & Shields, J. C. 1999, in Quasars and Cosmology, ed. G. Ferland, & J. Baldwin, ASP Conf. Ser., 162, 235
Ostriker, J. P., & Ciotti, L. 2005, Phil. Trans. Roy. Soc., Part A, 363, 1828, 667
Padovani, P., & Matteucci, F. 1993, ApJ, 416, 26
Peletier, R. F., & Balcells, M. 1996, AJ, 111, 2238
Peletier, R. F., Balcells, M., Davies, R. L., et al. 1999, MNRAS, 310, 703
Peterson, B. M., 2003, in Active Galactic Nuclei: from central engine to host galaxy, ed. S. Collin, F. Combes, & I. Shlosman, ASP Conf. Ser., 290, 43
Petitjean, P., & Srianand, R. 1999, A&A, 345, 73
Pipino, A., Matteucci, F., Borgani, S., & Biviano, A., 2002, NewA, 7, 227
Pipino, A., D'Ercole, A., & Matteucci, F. 2007, to appear in Formation and Evolution of Galaxy Bulges, ed. M. Bureau, E. Athanassoula, & B. Barbuy, IAU Symp., 245 [arXiv:0709.0658]
Rich, R. M., & Origlia, L. 2005, ApJ, 634, 1293
Rodríguez-Ardila, A., Contini, M., & Viegas, S. M. 2005, MNRAS, 357, 220
Romano, D., Silva, L., Matteucci, F., & Danese, L. 2002, MNRAS, 334, 444
Salpeter, E. E. 1955, ApJ, 121, 161
Sarzi, M., Shields, J. C., Pogge, R. W., & Martini, P. 2007, ed. R. F. Peletier, & A. Vazdekis, to appear in Stellar Populations as Building Blocks of Galaxies, IAU Symp., 241 [arXiv:astro-ph/0703794]
Sazonov, S. Yu., Ostriker, J. P., Ciotti, L., & Sunyaev, R. A. 2005, MNRAS, 358, 168
Scannapieco, E., Silk, J., & Bouwens, R. 2005, ApJ, 635, L13
Schmitt, H. R., Storchi-Bergmann, T., & Baldwin, J. A. 1994, ApJ, 423, 237
Shields, G. A., Gebhardt, K., Salviander, S., et al. 2003, ApJ, 583, 124
Storchi-Bergmann, T. 1991, MNRAS 249, 404
Storchi-Bergmann, T., & Pastoriza, M. G. 1989, ApJ, 347, 195
Storchi-Bergmann, T., Bica, E., & Pastoriza, M. G. 1990, MNRAS, 245, 749
Storchi-Bergmann, T., Wilson, A. S., & Baldwin, J. A. 1996, ApJ, 460, 252
Thomas, D., & Davies, R. L. 2006, MNRAS, 366, 510
Thomas, D., Maraston, C., & Bender, R. 2002, Ap&SS, 281, 371
Thompson, K. L., Hill, G. J., & Elston, R. 1999, ApJ, 515, 487
Tinsley, B. 1980, FCPh, 5, 287
Tremaine, S., Gebhardt, K., Bender, R., et al. 2002, ApJ, 574, 740
Turner, T. J., George, I., & Netzer, H. 1999, ApJ, 526, 52
Ulrich, M. H., Comastri, A., Komossa, S., & Crane, P. 1999, A&A, 350, 816
Van Loon, J. T., Gilmore, G. F., Omont, A., et al. 2003, MNRAS, 338, 857
Verner, E., Bruhweiler, F., Verner, D., Johansson, S., & Gull, T. 2003, ApJ, 592, L59
Wandel, A. 1999, ApJ, 519, L39
Wandel, A., Peterson, B. M., & Malkan, M. A. 1999, ApJ, 526, 579
Wang, R., & Wu, X. B. 2005, ChJAA, 5, 299
Warner, C., Hamann, F., & Dietrich, M. 2003, ApJ, 596, 72
Wills, B. J., Shang, Z., & Yuan, J. M. 2000, NewAR, 44, 511
Wu, X. B., & Han, J. L. 2001, A&A 380, 31
Yee, H. K. C. 1983, ApJ, 473, 713
Yu, Q., & Tremaine, S. 2002, MNRAS, 335, 965
Zoccali, M., Renzini, A., Ortolani, S., et al. 2003, A&A, 399, 931
Zoccali, M., Lecureur, A., Barbuy, B., et al. 2006, A&A, 457, L1